Helsinki University of Technology Radio Laboratory Publications
Teknillisen korkeakoulun Radiolaboratorion julkaisuja
Espoo, June 2007 REPORT S 289

STUDIES ON AN AMPLITUDE HOLOGRAM AS THE COLLIMATOR IN A SUBMILLIMETER-WAVE COMPACT ANTENNA TEST RANGE

Tomi Koskinen

Dissertation for the degree of Doctor of Science in Technology to be presented with due permission for public examination and debate in Auditorium S1 at Helsinki University of Technology (Espoo, Finland) on the 20th of June 2007 at 12 o'clock noon.

Helsinki University of Technology
Department of Electrical and Communications Engineering
Radio Laboratory

Teknillinen korkeakoulu
Sähkö- ja tietoliikennetekniikan osasto
Radiolaboratorio

Distribution:
Helsinki University of Technology
Radio Laboratory
P.O. Box 3000
FI-02015 TKK
Tel. +358-9-451 2218
Fax. +358-9-451 2152

ISBN 978-951-22-8795-6 (printed)
ISBN 978-951-22-8796-3 (pdf)
URL: http://lib.tkk.fi/Diss/2007/isbn9789512287963

ISSN 1456-3835

Multiprint Oy / Otamedia
Espoo 2007

HELSINKI UNIVERSITY OF TECHNOLOGY
P. O. BOX 1000, FI-02015 TKK
http://www.tkk.fi

ABSTRACT OF DOCTORAL DISSERTATION

Author Tomi Koskinen

Name of the dissertation

Studies on an Amplitude Hologram as the Collimator in a Submillimeter-Wave Compact Antenna Test Range

Date of manuscript February 6, 2007 | Date of the dissertation June 20, 2007

☐ Monograph ☒ Article dissertation (summary + original articles)

Department Electrical and Communications Engineering
Laboratory Radio Laboratory
Field of research Radio Engineering
Opponents Assistant Professor Amr M. E. Safwat and Dr. Arttu Luukanen
Supervisor Professor Antti V. Räisänen
Instructor Dr. Juha Ala-Laurinaho

Abstract

This thesis is based on the research work, the objective of which has been to develop a hologram-based compact antenna test range (CATR) for submillimeter wavelengths. Such a measurement facility is needed for testing antennas of, e.g., astronomical and Earth observation satellites. The further objective has been to improve electrical characteristics of the hologram, as well as its manufacturing properties. The hologram studied in this thesis is a slot pattern processed on a thin metal-plated Mylar film and it is used as a transmission-type collimating element.

A hologram-based CATR was designed and constructed for 322 GHz and was used for testing a 1.5 meter reflector antenna (Admirals RTO). A hologram of 3 meters in diameter was soldered together from three pieces, which were manufactured on 50 μm-thick copper-plated Mylar film by using laser-exposure and wet-etching. Partly due to manufacturing errors, the measured quiet-zone amplitude and phase deviations were appr. 1.2 dB and 250° within a region of 1.5 meters in diameter. The effect of these deviations on antenna measurement results was estimated by simulations.

Feasibility of the hologram for 650 GHz has also been studied. Laser-exposure and wet-etching has been found to be a potentially suitable manufacturing method for frequencies up to 1000 GHz. The 50 μm Mylar film is a suitable material for frequencies up to 650 GHz, but at higher frequencies the film has to be thinner to avoid resonances inside the film. The 25 μm Mylar film is estimated to be suitable for frequencies up to 1000 GHz.

According to studies at 310 GHz, the hologram works well also as a reflection-type element. In the reflection-type setup, the power loss of the hologram is appr. 7.4 dB that is 4 dB lower than that in the transmission-type setup.

Using a shaped beam for illumination has been studied at 310 GHz. A hologram pattern designed for such an illumination can be simplified from one designed for a conventional horn illumination. A simplified hologram pattern is easier to manufacture and it is more robust against manufacturing errors. In addition, its polarization properties are significantly improved: operation at the horizontal polarization is possible and cross-polarization is reduced substantially. Earlier, the operation of the hologram has been possible only at the vertical polarization. According to these studies, it appears that by using a shaped illumination the operation can be designed to be almost independent of polarization.

Keywords Hologram, compact antenna test range, CATR, submillimeter waves

ISBN (printed) 978-951-22-8795-6 | ISSN (printed) 1456-3835
ISBN (pdf) 978-951-22-8796-3 | ISSN (pdf)
ISBN (others) | Number of pages 70 + appendix 86

Publisher Helsinki University of Technology, Radio Laboratory

Print distribution Helsinki University of Technology, Radio Laboratory

☒ The dissertation can be read at http://lib.tkk.fi/Diss/2007/isbn9789512287963

TEKNILLINEN KORKEAKOULU PL 1000, 02015 TKK http://www.tkk.fi	VÄITÖSKIRJAN TIIVISTELMÄ

Tekijä Tomi Koskinen

Väitöskirjan nimi

Tutkimuksia amplitudihologrammin käytöstä kollimaattorina alimillimetriaaltoalueen kompaktissa antennimittauspaikassa

Käsikirjoituksen jättämispäivämäärä 6.2.2007	Väitöstilaisuuden ajankohta 20.6.2007

☐ Monografia ☒ Yhdistelmäväitöskirja (yhteenveto + erillisartikkelit)

Osasto	Sähkö- ja tietoliikennetekniikan osasto
Laboratorio	Radiolaboratorio
Tutkimusala	Radiotekniikka
Vastaväittäjät	Apulaisprofessori Amr M. E. Safwat ja FT Arttu Luukanen
Työn valvoja	Professori Antti V. Räisänen
Työn ohjaaja	TkT Juha Ala-Laurinaho

Tiivistelmä

Tämä väitöskirja pohjautuu tutkimustyöhön, jonka tavoitteena on ollut kehittää hologrammiin perustuva kompakti antennimittauspaikka alimillimetriaaltoalueelle. Tällaista mittauspaikkaa tarvitaan mm. astronomisten ja Maan ilmakehää luotaavien satelliittien antennien testauksessa. Lisätavoitteena on ollut parantaa hologrammin ominaisuuksia niin sähköisesti kuin valmistusteknisestikin. Tässä tutkimuksessa käsitelty hologrammi on ohuelle, metalloidulle Mylar-kalvolle valmistettu rakokuvio, joka toimii läpäisytyyppisenä kollimoivana elementtinä.

Hologrammiin perustuva kompakti antennimittauspaikka suunniteltiin ja rakennettiin taajuudelle 322 GHz ja sitä käytettiin 1,5 metrisen heijastinantennin (Admirals RTO:n) testaukseen. Halkaisijaltaan 3-metrinen hologrammi juotettiin yhteen kolmesta palasta, jotka oli valmistettu 50 μm:n paksuiselle kuparoidulle Mylar-kalvolle käyttäen laservalotusta ja märkäetsausta. Johtuen mm. hologrammin valmistusvirheistä mitattu hiljaisen alueen amplitudi- ja vaihevaihtelu oli n. 1,2 dB ja 250° 1,5 metrin kokoisella alueella. Tämän vaikutusta antennimittauksiin arvioitiin simuloinnein.

Myös hologrammin soveltuvuutta 650 GHz:n taajuudelle tutkittiin. Laservalotus ja märkäetsaus on havaittu tarkkuudeltaan sopivaksi valmistusmenetelmäksi mahdollisesti jopa 1000 GHz:n taajuudelle asti. 50 μm:n Mylar-kalvo on sopiva materiaali aina taajuudelle 650 GHz asti, mutta suuremmilla taajuuksilla kalvon on oltava ohuempi, jotta sen sisälle ei syntyisi resonansseja. 25 μm:n Mylar-kalvon on arvioitu olevan sopiva aina 1000 GHz:in asti.

310 GHz:lla tehtyjen tutkimusten mukaan hologrammi toimii hyvin myös heijastustyyppisenä elementtinä. Tällöin hologrammin tehohäviö on noin 7,4 dB, mikä on 4 dB vähemmän kuin häviö läpäisytyyppisessä toiminnassa.

Muotoillun keilan käyttöä hologrammin valaisuun tutkittiin 310 GHz:lla. Muotoillulle valaisulle suunniteltu hologrammikuvio on yksinkertaisempi kuin tavalliselle torviantennin valaisulle suunniteltu kuvio; yksinkertaisempi kuvio on helpompi valmistaa ja se sietää enemmän valmistusvirhettä. Myös sen polarisaatio-ominaisuudet ovat huomattavasti paremmat: toiminta myös vaakapolarisaatiolla on mahdollista ja ristipolarisaatiotaso laskee merkittävästi. Aiemmin hologrammin toiminta on ollut mahdollista vain pystypolarisaatiolla. Tutkimusten mukaan muotoiltua valaisua käyttäen hologrammin toiminta on mahdollista suunnitella lähes riippumattomaksi polarisaatiosta.

Asiasanat Hologrammi, kompakti antennimittauspaikka, alimillimetriaallot	
ISBN (painettu) 978-951-22-8795-6	ISSN (painettu) 1456-3835
ISBN (pdf) 978-951-22-8796-3	ISSN (pdf)
ISBN (muut)	Sivumäärä 70 + liitteet 86

Julkaisija Teknillinen korkeakoulu, Radiolaboratorio

Painetun väitöskirjan jakelu Teknillinen korkeakoulu, Radiolaboratorio

☒ Luettavissa verkossa osoitteessa http://lib.tkk.fi/Diss/2007/isbn9789512287963

Preface

These years in the Radio Laboratory at TKK have been enjoyable. I started my scientific career as a trainee in 1999, I got my Master's in 2001 and then my Licentiate's in 2004. I started in the Hologram project during my Master's thesis. Working in the Radio Laboratory has been rewarding in many ways and my excellent workmates have made possible to keep up a good spirit even during hard work - Thus, I would like to give my warmest thanks to you all.

I am very grateful to my supervisor, Professor Antti Räisänen, for giving me the opportunity to work in the Radio Laboratory and to write this thesis. I highly appreciate all the guidance, support, and the excellent resources he has provided during my work. I am thankful to my workmates in the Hologram group for the wonderful years we have spent together. Especially, I would like to thank Doctors Juha Ala-Laurinaho, Janne Häkli, Anne Lönnqvist, Juha Mallat, Jussi Säily, and Ville Viikari for the smooth co-operation, which made possible these magnificent research results ending up as tens of international journal and conference publications. I would like to give additional thanks to my instructor, Juha Ala-Laurinaho, for useful comments on this thesis. I am also thankful to other co-authors and co-workers, as well to Mr. Eino Kahra for building mechanical instruments for our hologram experiments.

I would like to thank Distinguished Professor Yahya Rahmat-Samii from UCLA and Dr. James C. Wiltse from Georgia Tech for pre-examining my thesis. I highly appreciate all the effort they have put into reading this thesis through within a very tight schedule.

I am grateful to Finnish foundations - Finnish Cultural Foundation, Foundation of the Finnish Society of Electronic Engineers, Jenny and Antti Wihuri Foundation, and Nokia Foundation - for the significant support they have given me over these years. Also, I would like to thank CSC - Finnish IT Center for Science - for access to their supercomputer to carry out calculations.

I am also very grateful to my parents and three brothers who have always encouraged me and have eagerly waited for this moment. Warm thanks also to my friends outside the Radio Laboratory for a great support.

Tomi Koskinen
Espoo, May 30, 2007

Contents

List of Publications

This thesis consists of an overview and of the following publications, which are referred to in the text by their Roman numerals.

I A. Lönnqvist, T. Koskinen, J. Häkli, J. Säily, J. Ala-Laurinaho, J. Mallat, V. Viikari, J. Tuovinen, and A. V. Räisänen, "Hologram-based compact range for submillimeter-wave antenna testing," *IEEE Transactions on Antennas and Propagation*, vol. 53, no. 10, pp. 3151–3159, Oct. 2005.

II J. Häkli, T. Koskinen, A. Lönnqvist, J. Säily, V. Viikari, J. Mallat, J. Ala-Laurinaho, J. Tuovinen, and A. V. Räisänen, "Testing of a 1.5-m reflector antenna at 322 GHz in a CATR based on a hologram," *IEEE Transactions on Antennas and Propagation*, vol. 53, no. 10, pp. 3142–3150, Oct. 2005.

III J. Salo, J. Meltaus, E. Noponen, M. M. Salomaa, A. Lönnqvist, T. Koskinen, V. Viikari, J. Säily, J. Häkli, J. Ala-Laurinaho, J. Mallat, and A. V. Räisänen, "Holograms for shaping radio-wave fields," *Journal of Optics A: Pure and Applied Optics*, vol. 4, no. 5, pp. S161–S167, Sep. 2002.

IV T. Koskinen, V. Viikari, J. Häkli, A. Lönnqvist, J. Ala-Laurinaho, J. Mallat, and A. V. Räisänen, "A reflection-type amplitude hologram as a collimating element in the compact antenna test range," in *Proc. 27th Annual Antenna Measurement Techniques Association (AMTA) Meeting & Symposium*, Newport, RI, USA, Oct. 30 – Nov. 4, 2005, pp. 417–421.

V T. Koskinen, J. Mallat, A. Lönnqvist, J. Säily, J. Häkli, J. Ala-Laurinaho, J. Tuovinen, and A. V. Räisänen, "Performance of a small 650 GHz hologram," in *Digest of the 2003 IEEE International Antennas and Propagation Symposium*, Columbus, OH, USA, June 22–27, 2003, vol. 3, pp. 532–535.

VI T. Koskinen, J. Ala-Laurinaho, J. Säily, A. Lönnqvist, J. Häkli, J. Mallat, J. Tuovinen, and A. V. Räisänen, "Experimental study on a hologram-based compact antenna test range at 650 GHz," *IEEE Transactions on Microwave Theory and Techniques*, vol. 53, no. 9, pp. 2999–3006, Sep. 2005.

VII J. Häkli, T. Koskinen, J. Ala-Laurinaho, and A. V. Räisänen, "Dual reflector feed system for hologram-based compact antenna test range," *IEEE Transactions on Antennas and Propagation*, vol. 53, no. 12, pp. 3940–3948, Dec. 2005.

VIII T. Koskinen, J. Häkli, J. Ala-Laurinaho, A. Lönnqvist, V. Viikari, J. Mallat, and A. V. Räisänen, "Study on the dual polarized operation of the hologram based compact antenna test range," in *Proc. 28th ESA Antenna*

Workshop on Space Antenna Systems and Technologies, ESTEC, Noordwijk, The Netherlands, May 31 – June 3, 2005, pp. 401–406.

IX T. Koskinen, J. Ala-Laurinaho, J. Häkli, and A. V. Räisänen, "Studies on an amplitude hologram as a submillimeter-wave collimator at circular polarisation," in *Proc. European Conference on Antennas & Propagation (EuCAP)*, Nice, France, Nov. 6–10, 2006, CD-ROM, ISBN: 92-9092-937.

The author of this thesis has also authored or co-authored 32 other articles [1–32] relevant to the topic of this thesis.

Author's contribution

Publication I The author designed and simulated the hologram and measured the manufacturing accuracy of the hologram. In co-operation with Dr. Anne Lönnqvist, the author developed the soldering method for joining the hologram pieces. The author simulated the effects of manufacturing errors of the hologram pattern. The author participated in the development and testing of the compact antenna test range. Dr. Jussi Tuovinen and Prof. Antti Räisänen supervised the work.

Publication II The author participated in the design, preparation and execution of the antenna measurements. Dr. Jussi Tuovinen and Prof. Antti Räisänen supervised the work.

Publication III The author simulated the full horizontal radiation pattern of the hologram. He also participated in writing and revision of the publication. Prof. Martti Salomaa, Dr. Juha Ala-Laurinaho, Dr. Juha Mallat, and Prof. Antti Räisänen supervised the work.

Publication IV The author has provided the main contribution to this publication. The author designed and simulated the hologram. He measured the quiet-zone field in co-operation with Dr. Juha Ala-Laurinaho and Dr. Juha Mallat. The author analyzed the measurement results and prepared the publication. The antenna radiation pattern measurements were done in co-operation with the author and Mr. Ville Viikari. Prof. Antti Räisänen supervised the work. The other authors participated in the development of this work.

Publication V The author has provided the main contribution to this publication. The author designed and simulated the hologram and prepared the publication. He made the quiet-zone tests in co-operation with Dr. Juha Mallat. Dr. Juha Ala-Laurinaho, Dr. Jussi Tuovinen, and Prof. Antti Räisänen supervised the work. The other authors participated in the development of this work.

Publication VI The author has provided the main contribution to this publication. The author designed and simulated the holograms and measured the manufacturing accuracy of the holograms. He analyzed the quiet-zone test results and prepared the publication. The author made the quiet-zone tests in co-operation with Dr. Juha Ala-Laurinaho and Dr. Jussi Säily. Dr. Anne Lönnqvist and Dr. Janne Häkli participated in the development of this work. Dr. Juha Mallat, Dr. Jussi Tuovinen, and Prof. Antti Räisänen supervised the work.

Publication VII The author designed and simulated the holograms. He also measured the manufacturing accuracy of the holograms and simulated the effect of hologram manufacturing inaccuracies. Dr. Juha Ala-Laurinaho and Prof. Antti Räisänen supervised the work.

Publication VIII The author has provided the main contribution to this publication. The author designed and simulated the holograms and prepared the publication. The measurements were done by Dr. Janne Häkli. Dr. Juha Mallat, Dr. Juha Ala-Laurinaho, and Prof. Antti Räisänen supervised the work. The other authors participated in the development of this work.

Publication IX The author has provided the main contribution to this publication. The author designed and simulated the holograms and prepared the publication. Dr. Juha Ala-Laurinaho has done cross-polarization simulations. Dr. Janne Häkli and Prof. Antti Räisänen supervised the work.

List of Abbreviations

The following abbreviations are used in the overview of this thesis.

ABmm	AB Millimètre
AUT	Antenna-Under-Test
CATR	Compact Antenna Test Range
CGH	Computer-Generated Hologram
DLR	Deutsches Zentrum für Luft- und Raumfahrt
DRFS	Dual Reflector Feed System
ESA	European Space Agency
ESTEC	European Space Technology Centre
FDTD	Finite Difference Time Domain
FFT	Fast Fourier Transform
HFI	High Frequency Instrument
IR	Infrared
ISS	International Space Station
JAXA	Japan Aerospace Exploration Agency
MilliLab	Millimetre Wave Laboratory of Finland
MVNA	Millimeter-wave Vector Network Analyzer
NASA	National Aeronautics and Space Administration
NICT	National Institute of Information and Communications Technology
PCB	Printed Circuit Board
PEC	Perfect Electric Conductor
PML	Perfectly Matched Layer
PO	Physical Optics
p-p	peak-to-peak
RCS	Radar Cross-Section
rms	root mean square
RTO	Representative Test Object
SNSB	Swedish National Space Board
Submm	Submillimeter
THz	Terahertz, 1 THz is 1000 GHz or 10^{12} Hz
TKK	Teknillinen korkeakoulu (Helsinki University of Technology, formerly HUT)

List of Symbols

The following symbols are used in the overview of this thesis.

a	transversal offset (m)
a_w	weight function
A	amplitude modulation
b	parameter
c_0	speed of light in vacuum, $2.99792458 \cdot 10^8$ m/s
D	diameter of hologram (m)
E_{in}	incident electric field (V/m)
E_x, E_y, E_z	electric field components (V/m)
f	frequency (Hz)
f_1	focal distance (m)
f_2	quiet-zone distance (m)
H_{in}	incident magnetic field (A/m)
H_x, H_y, H_z	magnetic field components (A/m)
L_{free}	free-space loss
r_{far}	far-field distance (m)
r_{near}	near-field distance (m)
T	transmission
T_B	binary transmission
x, y, z	coordinates in the goal field (i.e., in the quiet-zone field) (m)
x', y', z'	coordinates in the plane of the hologram (m)
α	feed rotation angle
δ_{Cu}	skin depth of copper (m)
ϵ_r	relative permittivity
η_0	wave impedance of vacuum, 376.73 Ω
θ	elevation angle, propagation angle
λ	wavelength (m)
μ_0	permeability of vacuum $4\pi{\cdot}10^{-7}$ Vs/Am
ν	spatial carrier frequency (1/m)
σ_{Cu}	conductivity of copper, $5.8{\cdot}10^7$ S/m
ϕ	azimuth angle
ψ	phase
Ψ	phase modulation
ψ_e	extra phase term

1 Introduction

In this chapter, the background and motivation for the research topic of this thesis are given. Scientific research at submillimeter wavelengths is briefly discussed in Sections 1.1 and 1.2. Section 1.3 summarizes the scope and contents of this thesis and Section 1.4 highlights the new scientific results obtained in this thesis work.

1.1 Scientific research at submillimeter waves

The submillimeter-wave range lies between the conventional microwave and optical (infrared) regions, covering the wavelengths 1000–100 μm. The corresponding frequency range (300 GHz–3 THz) is also known as the terahertz range [33, 34]. Despite a great general interest in the submillimeter-wave range, this range is one of the latest regions of the electromagnetic spectrum still not fully explored or utilized by the scientists and engineers. Partly, this has been due to a limited atmospheric transparency, which has prevented large commercial exploitation of this range, but also due to difficulties in construction of transmitters, receivers, and high-accuracy reflector antennas, which has made operation at submillimeter wavelengths very challenging. In recent years, technological progress has, however, brought this electromagnetic range closer to us, which can be seen, for example, as a growing number of scientific submillimeter-wave space missions.

The scientific interest in the submillimeter-wave range arises from the fact that nowhere else in the electromagnetic spectrum can we collect so much information about the universe [35,36]. Approximately one-half of the total luminosity and 98 % of the photons emitted since the Big Bang lie in the submillimeter and far-infrared regions [33]. A wide variety of molecules (e.g., water, oxygen, carbon monoxide, nitrogen) have thermal emission lines in the submillimeter-wave range. Therefore, valuable information about the chemical and physical structure of galaxies, stars, and intergalactic and interstellar media is available in the submillimeter-wave range. Astronomical observations in the submillimeter-wave range can also give us information about the early stages of the universe from the post-big-bang era. In addition, probing Earth's atmosphere with submillimeter-wave instruments can give useful information about our planet for meteorological and climatological purposes. Chemical compounds causing ozone depletion and global-warming can be traced with the help of remote sensing satellites. Space explorers equipped with submillimeter-wave instruments can also be sent to study the atmospheric conditions of our neighboring planets and small bodies, such as asteroids, moons, and comets.

On-ground astronomical measurements at submillimeter waves are interfered by the Earth's atmosphere [35]. For electromagnetic waves up to millimeter waves (0–300 GHz), the atmosphere is almost completely transparent discarding a few oxygen and water absorption lines. At submillimeter wavelengths, however, there are only a few useful windows, where the transparency is reasonable: around frequencies 400, 500, 650, and 850 GHz. Elsewhere in the submillimeter-wave range, the transparency is reduced by water absorption lines making the atmosphere opaque. Figure 1.1 shows the computed atmospheric opacity as a function of frequency for a 1 km horizontal test path through moist air [37]. Due to this limited atmospheric transparency, astronomical observations at submillimeter wavelengths have to be done from very-high-altitude platforms, such as mountain tops, aircrafts, and balloons, where the water vapor content is low. Preferably, observations are done from satellite telescopes outside the Earth's atmosphere. Studying gases in the stratosphere and upper troposphere is also best done from satellites. Naturally, missions become far more demanding and expensive, when on-ground solutions cannot be used, but measurements have to be carried out from satellites.

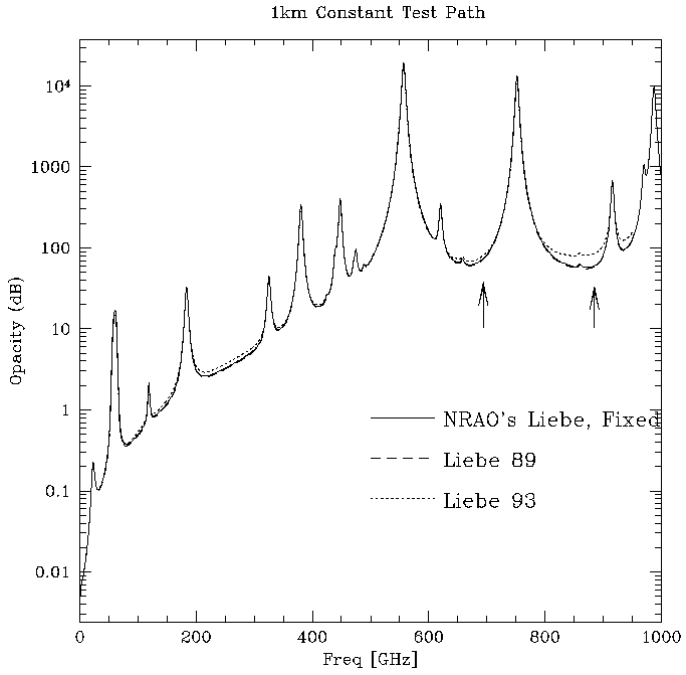

Figure 1.1: Computed atmospheric opacity as a function of frequency for a 1 km horizontal test path through moist air [37].

Some recent and future submillimeter-wave astronomy and atmospheric missions are collected in Tables 1.1 and 1.2 with a short description. More information can be found from the references given in the tables. For each mission listed, the approximate operational frequency range of the high frequency instruments (HFI) is given, as well as the diameter (or the maximum dimension) of the antenna.

Table 1.1: Astronomy missions at submillimeter wavelengths in chronological order.

Mission	Host	Description	Status (launch in)	HFI (GHz)	Antenna (m)
SWAS [38, 39]	NASA	Space telescope	1998	490, 550	0.68
Odin [40]	SNSB	Space telescope, remote sensing	2001	119–581	1.1
Rosetta/ MIRO [41, 42]	ESA	Comet explorer	2004	190–564	0.3
BLAST [43, 44]	NASA	Balloon-borne telescope	2005	600–1200	2
SOFIA [45, 46]	NASA, DLR	Airborne telescope	2006	187–IR	2.5
Herschel [47]	ESA	Space telescope	2007	480–2700	3.5
Planck [47, 48]	ESA	Space telescope	2007	100–857	1.5
SPIRIT [49]	NASA	Space interferometric telescope	2010–20	600–7500	1–3
SPECS [49, 50]	NASA	Space interferometric telescope	2010–20	600–7500	3

Table 1.2: Atmospheric missions at submillimeter wavelengths in chronological order.

Mission	Host	Description	Status (launch in)	HFI (GHz)	Antenna (m)
Aura/ EOS MLS [51]	NASA	Space limb sounder	2004	118–640	1.6
BSMILES [52]	NICT, JAXA	Balloon-borne limb sounder	2004	624–639	0.3
TELIS [53, 54]	DLR	Balloon-borne limb sounder	2006	500–1800	0.27
SMILES [55, 56]	NICT, JAXA	Limb sounder on ISS	2008	624–650	0.4
MASTER [57, 58]	ESA	Space limb sounder	unknown	199–348	2.2
SOPRANO [57, 58]	ESA	Space limb sounder	unknown	498–956	1

The antennas typically used in these missions are paraboloidal reflectors, which give high directivity, i.e., high angular resolution. In the listed missions, the reflector diameters vary from 0.27 m to 3.5 m. Increasing the reflector diameter makes the main beam sharper, and thus improves angular resolution. Very high angular resolution is needed in probing inside star systems and galaxies, and for example, when high spatial accuracy is desired in atmospheric measurements. The surface of the reflector has to be shaped accurately to avoid side lobes and deformation of the main beam, which degrade measurement accuracy. Usually, these reflectors together with their feed systems represent state-of-the-art technology, and thus manufacturing of these antennas is very demanding, which increases the risk of failure [48, 59].

1.2 Submillimeter-wave antenna testing

Undoubtedly, the correct operation of the antenna has to be verified by extensive tests to avoid unsuccessful missions and a huge loss of money. Especially in space applications, possible faults have to be detected and fixed before the launch, as correcting them afterwards is very difficult or not possible at all. Perhaps, the most crucial electrical test done for the antenna is the measurement of its radiation pattern. The antenna radiation pattern tells directly, how the antenna receives electromagnetic radiation from different directions. Unfortunately, the current measurement facilities used at lower frequencies face difficulties in performing successfully in the submillimeter-wave range. Therefore, existing facilities have to be upgraded for submillimeter wavelengths or new methods have to be introduced, so that also future submillimeter-wave antennas can be tested conveniently and reliably.

A compact antenna test range (CATR) [60] is perhaps the most potential method for testing large aperture (reflector) antennas at submillimeter wavelengths [61, 62]. In the CATR, a collimating element (collimator) is used for generating a planar wavefront so that the antenna radiation pattern can be measured in a relatively small space indoors. Conventionally, the collimator is a set of two shaped reflectors. However, at submillimeter wavelengths, the use of reflectors becomes difficult due to tight manufacturing tolerances.

In the Radio Laboratory of the Helsinki University of Technology (TKK), a transmission-type amplitude hologram has been used as the collimator [63]. A transmission-type amplitude hologram is a computer-generated slot pattern processed on a thin metal-plated dielectric film. The hologram has many advantages related to its planar structure and facilitated manufacturing, which makes it appealing to use at submillimeter wavelengths [62, 63]. Holograms have earlier been used successfully for antenna testing at millimeter wavelengths [64, 65].

1.3 Scope and contents of this thesis

This thesis focuses on the research work, the objective of which has been to upgrade the hologram-based CATR for the submillimeter-wave range. It presents also ways to improve significantly the properties of the hologram. The research work was carried out in the TKK Radio Laboratory.

The thesis is divided into two parts: an overview and nine scientific articles. Chapter 2 discusses the measurement problem of an electrically large antenna at submillimeter wavelengths. Different methods are considered to carry out radiation pattern measurements. Chapter 3 introduces the hologram-based CATR and the simulation method used in the hologram design. Chapter 4 presents the hologram-based CATRs built for submillimeter wavelengths: two transmission-type setups for 322 GHz [I,II] and 650 GHz [V,VI], and a reflection-type setup for 310 GHz [III,IV]. Chapter 5 considers how properties of the hologram can be improved [VII–IX]. Several improvements are possible, if the illumination of the hologram is shaped with a dual reflector feed system. The improvements include: better manufacturing properties, optimized operation at the horizontal and circular polarization, and reduced cross-polarization product. Chapter 6 gives the summary of the publications and Chapter 7 concludes the thesis and discusses briefly possible research topics in future.

1.4 New scientific results

In this thesis, the following new scientific results have been obtained:

1. A temporary and transportable hologram-based CATR was designed and built for 322 GHz [I] and was used for testing of a high-gain antenna [II].
2. A reflection-type hologram was studied at 310 GHz and was used for demonstrative antenna measurements [III,IV].
3. Feasibility of the hologram-based CATR for higher submillimeter-wave frequencies was studied and demonstrated at 650 GHz [V,VI].
4. A dual reflector feed system (DRFS) was used for illumination of holograms. According to the study, holograms designed for such an illumination have better manufacturing properties [VII] and improved operation at the horizontal feed polarization [VIII].
5. A hologram illuminated with a DRFS was designed for the circular polarization having significantly reduced cross-polarization product [IX].

2 Testing of electrically large antennas

This chapter discusses briefly the radiation of an antenna and introduces three widely-known methods used for antenna radiation pattern measurements. The feasibility of these methods for testing large submillimeter-wave antennas is considered.

2.1 Antenna radiation

Heinrich Hertz's experiments [66] with electromagnetic waves over one hundred years ago opened a door to radio science eventually leading to inventions such as the radio and mobile phone. From the early beginning, it has been clear that a suitable device is needed to transfer electromagnetic waves from the closed oscillator circuit to air or free space, and correspondingly, to collect them from air to the detector circuit. A device suitable for such a purpose is called an antenna.

In the antenna design process, an appropriate antenna type is chosen and its radiation properties (such as gain, beam width, polarization, and cross polarization) are optimized for the specific application [67–69]. What properties are stressed, depends on the application, for which the antenna is used. Hertz made his experiments mainly by using wire antennas, such as dipoles and loops. These antennas have low directivity and gain. He made experiments also with parabolic reflectors and showed that radio waves can be controlled similarly as optical waves. High directivity and gain, i.e., a narrow beam usually characterize this kind of antennas. Physical differences can be significant between different antenna types: the length of a dipole is typically of the order of a wavelength, whereas the diameter of a reflector antenna is from tens to thousands of wavelengths. Antennas of large size in wavelengths are called electrically large.

Nature of the electromagnetic field surrounding the antenna depends strongly on the distance from the antenna. Usually, the field generated by the antenna can be divided into three distinct regions: the reactive near-field region, the radiating near-field (Fresnel) region, and the far-field (Fraunhofer) region [67]. Although the field does not change abruptly, when the boundaries are crossed, the field in each region has a distinctive nature. How the field changes depends on the radiation characteristics of the antenna. In the immediate proximity of the antenna lies the reactive near-field region, where the reactive, non-radiating field components dominate. The reactive power associated to this field does not propagate away from the antenna, but oscillates in the vicinity of the antenna. For electrically small antennas (e.g., a small dipole), the approximate outer boundary of the reactive near-field region is

commonly taken to exist at a distance [67]

$$r_{near} = \lambda/2\pi \tag{2.1}$$

where λ is the wavelength. Perhaps, a more reasonable outer boundary would be $r_{near} = \lambda$ as given in [70] to ensure a sufficient distance. For antennas of appreciable electrical size, the outer boundary is commonly taken to exist at a distance [67]

$$r_{near} = 0.62\sqrt{D^3/\lambda} \tag{2.2}$$

where D is the largest dimension of the antenna.

The reactive field components decay faster with the distance than the radiating components. In the radiating near-field region, the radiating field components predominate and the angular field distribution is dependent on the distance from the antenna. The radial field components may be appreciable. If the antenna has a maximum dimension that is not large compared to the wavelength, this region may not exist. In the far-field region, the field components are essentially transverse and the angular field distribution is independent of the distance. For electrically large antennas, the approximate distance to the far-field region is given by [67]

$$r_{far} = 2D^2/\lambda. \tag{2.3}$$

An antenna (radiation) pattern represents the radiation properties of the antenna as a function of space coordinates. Radiation properties are, for example, amplitude (field strength), phase, and polarization. In most cases, the radiation pattern is determined in the far-field region and is represented in the standard spherical coordinate system, i.e., as a function of the directional coordinates θ and ϕ (elevation and azimuth angle) on a constant radius sphere [71]. Usually, only a few cuts of the radiation pattern are needed to give the most useful information about the radiation properties of the antenna. A pattern cut is obtained by fixing one of the angles (θ or ϕ) while varying the other. The most interesting pattern cuts are usually the horizontal and vertical cuts, which intersect the main beam of the antenna.

Most antennas are reciprocal, i.e., their receiving mode properties are identical to those of the transmitting mode. Such an antenna can be tested in either mode. The antenna is nonreciprocal, if it includes, for example, active or nonlinear elements.

In that case, its receiving mode and transmitting mode properties differ, and thus the antenna has to be tested in the same mode where it is intended to be used.

2.2 Antenna measurements

In the following, three antenna measurement methods are introduced. They are widely known and well established at microwave frequencies. Here, their suitability for testing of electrically large antennas at submillimeter wavelengths is considered.

2.2.1 Far-field method

If the antenna under test (AUT) is reciprocal, the ideal condition for measuring far-field radiation properties is to illuminate the antenna with a plane wave, which has uniform amplitude and phase. In the far-field method (which can be used also for nonreciprocal antennas), this condition is approximated by separating the AUT from the illumination source by a sufficient distance so that the curvature of the spherical phasefront produced by the source antenna is small over the aperture of the AUT. If the separation distance is equal to (2.3), then the maximum phase curvature is about 22.5° [67, 72]. In some cases, even a smaller phase curvature is desired for better measurement accuracy, and then the separation distance has to be larger than the one given by (2.3) [67, 73]. The source antenna is assumed to be electrically small, e.g., a horn antenna having an aperture of the order of a wavelength. To obtain the radiation pattern over a certain angular range, the AUT is rotated by an antenna positioner in the azimuth and elevation directions.

The far-field method is the most traditional way to carry out antenna measurements and it is widely used up to microwave frequencies. Unfortunately, at higher frequencies, the separation distance needed for large AUTs becomes very long, which complicates far-field measurements. Table 2.1 shows the far-field distance calculated from (2.3) for various aperture diameters and frequencies. It is obvious that the four last antennas can be tested only in an outdoor range due to the large separation distance needed. Outdoor measurements are susceptible to distortions from changing weather conditions and atmospheric inhomogeneities (temporal and spatial temperature, pressure, and humidity variations), which are possible in a long measurement distance. Also, ground reflections (multipath propagation) affect the measurement. However, the main reason that makes the far-field method impracticable for testing large submillimeter-wave antennas is the huge atmospheric attenuation (see Figure 1.1). At submillimeter wavelengths, where output powers of typical sources are very

limited [33], a sufficient dynamic range for ensuring accurate measurements is difficult to reach, when the propagation losses are high. Near water absorption lines in normal tropospheric conditions, atmospheric attenuation can be up to tens of thousands of decibels per kilometer, which definitely rules out the far-field measurements at those frequencies.

Table 2.1: Far-field distance for various aperture diameters and frequencies.

f (GHz)	λ (mm)	D (mm)	D/λ	r_{far} (m)
3	100	1000	10	20
10	30	250	8.3	4.2
10	30	1000	33.3	67
300	1	1000	1000	$2 \cdot 10^3$
1000	0.3	250	833.3	420
1000	0.3	1000	3333.3	$6.7 \cdot 10^3$
1000	0.3	3000	10000	$6 \cdot 10^4$

2.2.2 Near-field method

In the near-field method, the near field of the AUT is measured, from which the far-field is computed numerically by using the far-field transformation based on, e.g., the FFT (Fast-Fourier Transform) [67, 70, 74]. As measurements can be done in a small space indoors, the atmospheric conditions as well as the cleanliness of the test site can be controlled. Atmospheric inhomogeneities and attenuation do not cause significant disturbances in the near-field measurements.

The near-field amplitude and phase of the AUT is sampled with a probe antenna, such as a horn or an open waveguide end. This can be done over a plane, a cylinder, or a sphere. In the cylindrical measurement, the AUT is rotated in one direction and the probe is moved linearly by a scanner in the other direction. In the spherical measurement, the AUT is rotated in two directions. As the accurate rotation of large and heavy antennas is difficult, a planar near-field measurement is preferred, where only the probe antenna is moved in the scanner. The geometry of planar movement can be rectangular, plane-polar, or bi-polar [70, 75]. The most typical geometry is the rectangular geometry, where the probe is moved along the two orthogonal linear directions by using a xy-scanner. The planar near-field method suits well for high-gain (i.e., narrow-beam) antennas, which have a distinctive aperture.

The near-field measurement area has to be larger than the antenna aperture to ensure that all essential radiation emitted from the AUT is included in the far-field transformation. If the measurement area is insufficient, the angular range, where the far-field results are valid, is reduced [76]. The near-field samples have to be collected with a density that fulfills the Nyquist criterion, i.e., the distance of two adjacent sample points has to be less than $\lambda/2$ in the rectangular planar geometry. Otherwise, the data are aliased, which reduces the valid angular range of the far-field data [70, 76]. Due to a huge number of samples needed, the near-field measurement of large submillimeter-wave antennas can be very time consuming and take several days. Thus, a very high stability is required for the measurement system.

The radiation pattern of the probe antenna has to be taken into account in the far-field transformation, for which purpose special probe compensation methods have been developed [70]. Phase measurements at submillimeter wavelengths are very demanding. Flexing of RF cables during scanning causes phase errors, which have to be eliminated, e.g., by using a pilot signal based phase correction system [76–78]. Also, inaccurate movement of the probe, especially, non-planarity of the xy-scanner causes measurement errors, of which phase errors are the most significant ones. Reflections between the probe and the AUT can be significant and they have to be eliminated to avoid measurement errors [76]. Phaseless near-field methods are suggested to overcome difficulties met in phase measurements. In these methods, phase retrieval algorithms are used to find the near-field phase from the measured amplitude data [79, 80]. However, these methods are not yet well established for submillimeter-wave antenna testing.

The near-field method is applicable for testing large submillimeter-wave antennas. However, very high stability and accuracy is required for the measurement system that makes near-field measurements very demanding. The near-field method can give more information about the antenna than, for example, the far-field method; if the far-field pattern does not meet the required specifications, it may be possible to use the near-field data for further analysis to identify the problem in the antenna structure. The near-field method has been used, for example, at 640 GHz for testing NASA's EOS MLS, which has a 1.6 m reflector antenna [51].

2.2.3 Compact antenna test range

In a compact antenna test range (CATR), the plane wave needed for illumination of the AUT is produced from a spherical wave with a collimator [60]. The AUT is placed into the quiet-zone, which is a volume of the collimated wave having a high amplitude and phase planarity. Typical requirements for the quiet-zone field are that its amplitude and phase planarity should be within 1 dB and 10°, peak-to-peak [61].

As the collimation can be done in a short range, the CATR can be situated indoors, and thus the atmospheric conditions as well as the cleanliness of the test site can be controlled. In addition, the propagation losses are tolerable. The antenna radiation pattern is measured directly by rotating the AUT as in the far-field method. The main beam of a high-gain antenna can also be measured by moving the feed of the CATR in the transversal direction, which turns the propagation angle of the plane wave. Straightforward and relatively fast measurements make the CATR attractive for use at submillimeter wavelengths [61].

The collimator can be a reflector, a lens, an array, or a hologram. Conventionally, it is a reflector or a set of two reflectors [81–83] illuminated with a horn antenna in an offset geometry. Figure 2.1 shows the principle of a CATR based on a single-offset reflector. The offset geometry increases cross polarization, which is about –30 dB for a single-reflector CATR [81]. The cross polarization produced by the main reflector can be compensated by using an appropriate subreflector. In dual-reflector CATRs, the cross-polarization level is typically –40 dB or less [81, 82]. In addition, by using a dual or tri-reflector setup, the planarity and size of the quiet-zone can be increased significantly. In the tri-reflector setup, the main reflector is illuminated with a dual reflector feed system (DRFS) [84, 85]. The reflectors of the DRFS are essentially smaller than the CATR main reflector. Approximately, a quiet-zone of 70–75 % of the diameter of the main reflector is achievable by using a dual- or tri-reflector setup.

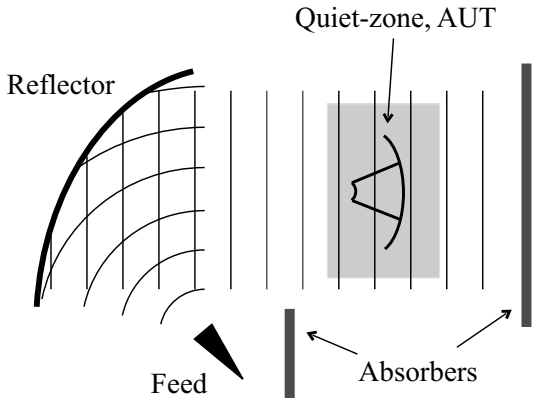

Figure 2.1: Principle of a single-reflector CATR with an offset feed.

If the edge illumination is high, the reflector edges may cause severe distortions to the quiet-zone field unless treated correctly. In the dual- and tri-reflector CATRs, edge diffraction can be reduced by tapering the illumination of the main reflector towards the edges. In addition, edge diffraction can be reduced by using serrated or rolled edges [67,86], or by placing resistive sheets (R-cards) in front of the edges [87].

The AUT has to fit completely inside the quiet-zone so that it can be measured reliably. Therefore, the main reflector of the CATR has to be clearly larger than the AUT. Manufacturing of large reflectors for submillimeter wavelengths is very difficult and expensive due to an extremely high surface accuracy requirement. The rms surface accuracy should be better than 0.01λ [71]. For example, at 1 THz it equals to 3 μm. Large reflectors have to be made from pieces, alignment and joining of which is a demanding task.

Reflectors operate over a wide frequency range. The minimum operation frequency is limited by the edge diffraction and the maximum operation frequency is limited by the surface accuracy. However, the feed has to be changed for each frequency band. Reflectors are used widely at millimeter wavelengths, but at higher frequencies their capability is limited by the high surface accuracy requirement. Reflector CATRs have been used for antenna testing at frequencies up to 320 GHz [88] and their capability has been investigated up to 500 GHz [82, 83, 89].

As it was mentioned earlier, also a lens and an antenna array can be used as the collimator. A CATR based on a planar waveguide array has been demonstrated at 12 GHz [90]. However, using arrays at submillimeter wavelengths is not reasonable due to very difficult manufacturing. As the lens is a transmission-type element, its surface accuracy requirement is eased by a factor of $\sqrt{2}/(\sqrt{\epsilon_r} - 1)$ from that of a reflector [81]. If the lens is manufactured of a low-permittivity dielectric material, the surface accuracy requirement is eased considerably. Lenses operate also over a wide frequency range, which is limited by the edge diffraction and the surface accuracy. Unfortunately, a lens made of a low-permittivity material becomes bulky and difficult to handle. In addition, an appropriate low-permittivity, high-homogeneity material is difficult to find. The hologram-based CATR is discussed in Chapter 3.

3 Hologram-based compact antenna test range

The concept of the radio-wave hologram is introduced in this chapter. Design, simulation, and manufacturing of a hologram are discussed. The chapter concentrates on the plane-wave generating amplitude hologram, which is used in the compact antenna test range. Its properties as a collimator are considered.

3.1 Introduction

Holography was invented in 1947 and after that holographic applications have spread over a wide range of engineering fields [91]. In general, holograms are understood as a three dimensional picture, for example, in a bank note or credit card. In traditional optical holograms, a photographic film is exposed to the interference pattern of two beams. One of the beams is scattered from the object and the other is a coherent reference beam coming directly from the light source that is typically a laser. When the film is illuminated with the reference beam, a holographic image of the object is seen.

Modern optical holograms are designed by computing the required diffractive structure numerically [92]. The holograms are manufactured by printing or etching the designed structure on a suitable substrate. This type of hologram is called computer-generated holograms (CGH) and they can be used to perform many kinds of optical operations, like beam focusing, beam splitting, and spatial filtering.

In the early 1990's, it was found in the Radio Laboratory of the Helsinki University of Technology that computer-generated radio-wave holograms could be used as a collimating element in the CATR [63]. Successful antenna tests carried out at 39 GHz and 119 GHz have verified the applicability of the hologram-based CATR at millimeter wavelengths [64, 65, 93]. After that, the focus has been on the development of the hologram-based CATR for submillimeter wavelengths [94], where the conventional reflector-based CATR has faced difficulties due to tight manufacturing tolerances as discussed in Section 2.2.3. Holograms have also been used to produce more complex beams than a plane wave: for example, experiments with radio-field vortices, bessel beams, and arbitrarily shaped beams have been demonstrated at submillimeter wavelengths (see [13, 95] and [III]).

To produce plane waves, two computer-generated hologram types have been investigated in the Radio Laboratory, namely amplitude and phase holograms. Both

hologram types are locally periodic diffraction gratings. However, their operation principle and structure are different: operation of the amplitude holograms is primarily based on amplitude modulation of the incident wave, whereas operation of the phase holograms is based on phase modulation. In the phase holograms, the effective electrical thickness of the hologram structure is locally varied, which causes the desired phase modulation [13, 18]. The phase holograms can be manufactured, for example, by milling a computer-generated groove pattern on a Teflon plate. These holograms have been used in scale-model radar cross-section (RCS) measurements [96]. However, in CATRs where large quiet-zones are needed, binary amplitude holograms are more suitable due to their simple structure, which makes it possible to construct large holograms relatively easily. The binary amplitude holograms are metal grating patterns etched on a thin metal-plated dielectric sheet [63]. This chapter concentrates on the binary amplitude holograms used in CATRs.

3.2 Hologram design

3.2.1 Binary transmission function

If the incident field is known, a binary amplitude hologram pattern can be generated to produce the desired goal field. In CATR applications, the incident field is the spherical-wave illumination, like a horn antenna illumination, and the goal field is the plane wave diffracted from the hologram. By a scalar theory, the hologram structure modulates the amplitude of the incident wave with a binary function that can have two values, 0 or 1. For example, a transmission-type binary amplitude hologram pattern consists of areas that allow the incident field go through undisturbed (transmission $T = 1$) or block the incident field completely (transmission $T = 0$). The binary transmission function, $T_B(x', y')$, that defines the hologram pattern can be formulated as follows [13, 63]

$$T_B(x', y') = \begin{cases} 0, & \text{if } 0 \leq \frac{1}{2}[1 + \cos\Psi(x', y')] \leq b \\ 1, & \text{if } b < \frac{1}{2}[1 + \cos\Psi(x', y')] \leq 1 \end{cases} \tag{3.1}$$

where

$$b = 1 - \frac{1}{\pi} \arcsin A(x', y'). \tag{3.2}$$

In the previous formulas, $A(x', y')$ is the amplitude modulation, $\Psi(x', y')$ is the phase modulation, and (x', y') are the coordinates in the plane of the hologram. The amplitude and phase modulation define the required amplitude and phase transformation from the incident field to the goal field. The amplitude modulation can be presented as follows

$$A(x', y') = \frac{a_w(x', y')}{|E_{in}(x', y')|} \tag{3.3}$$

where $|E_{in}(x', y')|$ is the normalized amplitude of the incident electric field $E_{in}(x', y')$ and $a_w(x', y')$ is a weight function, which is used to optimize the amplitude modulation.

The hologram can be designed to operate either on- or off-axis, i.e., the goal field can propagate from the hologram in a normal or oblique angle. However, the full control of the amplitude and phase is only possible, when the hologram is designed to operate off-axis. In the off-axis operation, the diffraction modes produced by the hologram are separated by a spatial carrier frequency and the goal field is carried by a non-zero diffraction order that is typically the first diffraction order. To separate the diffraction modes in the horizontal direction, the linear phase term $2\pi\nu x'$ is added to the phase modulation, i.e.,

$$\Psi(x', y') = \psi(x', y') + 2\pi\nu x' + \psi_e(x', y') \tag{3.4}$$

where ν is the spatial carrier frequency. The phase term $\psi(x', y')$ defines the phase transformation from the incident field to the goal field. If the goal field is a plane wave, $\psi(x', y')$ is the normalized phase of the incident field. The phase modulation can be optimized with the extra phase term $\psi_e(x', y')$, which is much smaller than $2\pi\nu x'$. For a nonzero ν, the first diffraction order leaves the hologram at an angle

$$\theta = \arcsin \nu\lambda. \tag{3.5}$$

Figure 3.1 shows an example of a binary amplitude hologram pattern, which produces a plane wave. The pattern consists of vertical, slightly curved, radio-wave transparent slots and non-transparent strips. Slots are shown in white and strips in black. Slots and strips are of the order of a wavelength in width and their number can be from hundreds to several thousands depending on the electrical size of the

hologram. The grating periodicity increases smoothly from left to right. The amplitude modulation is coded to the slot widths and the phase modulation to their locations. The amplitude of the transmitted field can be increased (decreased) by widening (narrowing) the slots locally according to the weight function $a_w(x', y')$. Correspondingly, the phase of the transmitted field can be shaped by tuning the locations of the slots according to the extra phase term $\psi_e(x', y')$. A local change in the transmitted field affects mainly locally the quiet-zone field, which makes optimization of the CATR hologram quite straightforward.

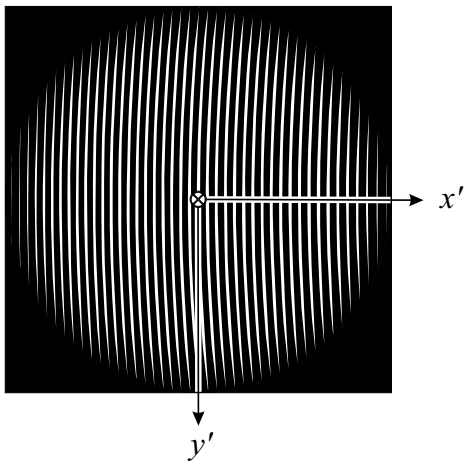

Figure 3.1: Binary amplitude hologram pattern used to produce a plane wave.

3.2.2 Hologram optimization

Figure 3.2 shows a transmission-type CATR setup. Typically, the propagation angle of the plane wave is designed to be $\theta = 33°$ in respect to the surface normal of the hologram. At this propagation angle, the quiet-zone can be optimized reasonably close to the hologram, however, avoiding disturbances from the zeroth order diffraction mode propagating perpendicularly from the hologram. The quiet-zone field is usually optimized at the distance three times the diameter of the hologram.

Figure 3.3 shows the full horizontal radiation pattern of a 1-m-diameter hologram simulated at 650 GHz [III]. The pattern is calculated for the vertical electric field polarization at a distance of 3 m from the hologram. The hologram is designed to form a plane wave that propagates at the angle 33° in respect to the surface normal. The transmitted field is seen in the angle range from $-90°$ to 90° and the reflected field is seen in the range above 90°. The flat peak at 147° is the reflected plane wave

that is located symmetrically with respect to the transmitted one. The transmitted and reflected zeroth order beams are seen at 0° and 180°, respectively.

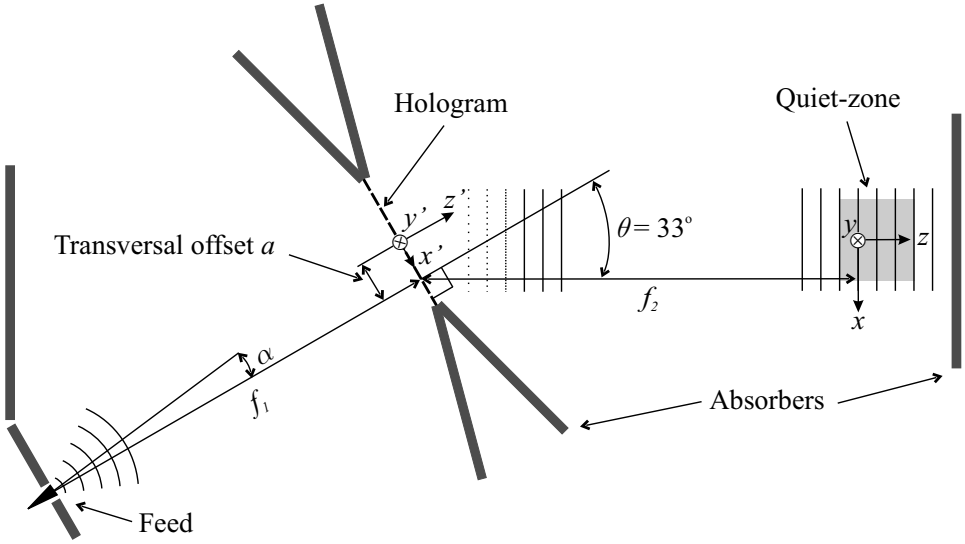

Figure 3.2: CATR based on a transmission-type hologram.

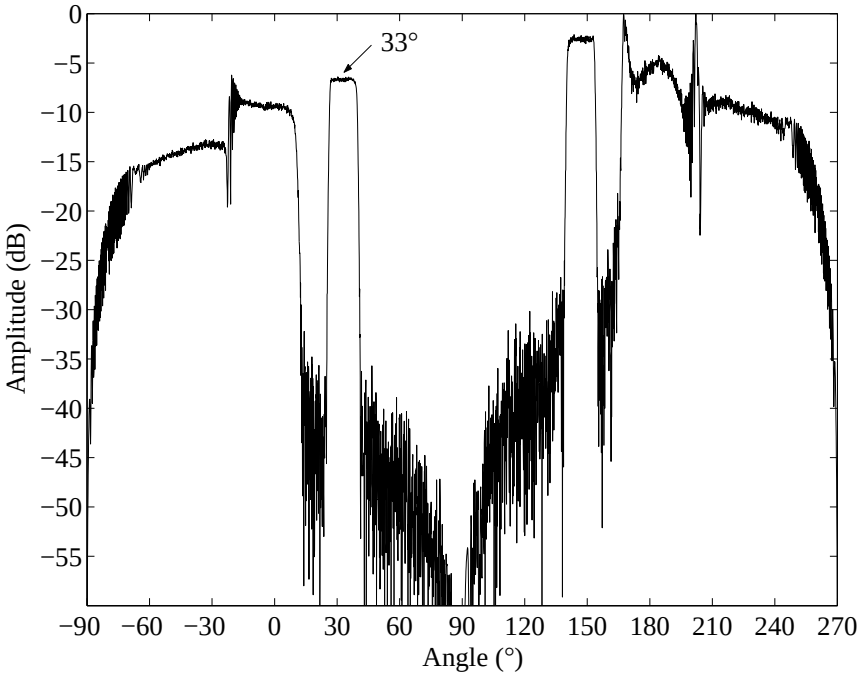

Figure 3.3: Full simulated horizontal radiation pattern of a 1-m-diameter hologram at 650 GHz. The transmitted plane wave is shown by an arrow.

An oblique propagation angle decreases the width of the quiet-zone in the horizontal direction. If the propagation angle is 33°, a circular hologram pattern produces an elliptical quiet-zone that is approximately $\cos 33° \approx 0.84$ times smaller in the horizontal direction than in the vertical direction. A circular quiet-zone can be produced with an elliptical hologram that is $1/0.84 \approx 1.2$ times wider in the horizontal direction than in the vertical direction. For such a hologram, the illuminating beam should be rather wide to ensure sufficient illumination over the whole hologram aperture. Moving the feed further away from the hologram makes the illumination more uniform.

Typically, holograms are illuminated with a corrugated horn antenna, which has a Gaussian beam. The optimal focal distance f_1 is a trade-off between the compactness of the CATR and the performance of the hologram. However, the focal distance has to be sufficiently large to keep the Gaussian shape of the illumination moderate, so that it can be compensated with the hologram. A large focal distance moderates also the spherical phase curvature of the illumination, which reduces the curvature of the slots and evens out the local variation of the grating periodicity. It has been found that the hologram operates better, when the variation of the grating periodicity is reduced. The variation of the grating periodicity can be further reduced by moving the feed from the optical axis to right (see the transversal offset a in Figure 3.2). To re-align the illumination, the feed has to be turned by the angle α towards the center of the hologram. If the diameter of the hologram is D, the focal distance is typically $3D$ and the transversal offset is 0.27–$0.35D$.

The edge illumination is high (up to –1.6 dB in [VI]), when the horn antenna is used as the feed. To eliminate diffraction fringes in the quiet-zone field, the transmission has to be tapered on the edges. This can be done by narrowing the slots towards the pattern edges like in Figure 3.1. As the transmission of the hologram structure is not purely binary but a complex function that depends strongly on the slot widths, on the incident-wave polarization, and also on the dielectric substrate, the actual operation of the hologram has to be verified by electromagnetic simulation. According to the simulation results, the hologram pattern is modified appropriately to fulfill the planarity requirements set for the quiet-zone field. Usually, only the amplitude weight function $a_w(x', y')$ in (3.3) is modified; the extra phase term $\psi_e(x', y')$ in (3.4) is rarely needed to correct a possible phase deviation. A typical phase deviation is such that it can be compensated by tuning the location of the feed slightly.

Operation of the hologram is optimized first on the plane $y = 0$, i.e., along the centerline of the hologram, and then the operation is verified on the other planes. If necessary, the hologram pattern can be locally modified in the y direction; usually, this is not necessary. The simulation of the hologram structure is discussed in Section 3.3.

3.3 Electromagnetic simulation

The electromagnetic modelling and analysis of the CATR hologram is based on the finite-difference time-domain (FDTD) method followed by the use of physical optics [63]. Due to the enormous size of the hologram and the numerous small-scale details (slots and strips), the direct electromagnetic analysis of an entire hologram pattern would require massive computing effort, even for supercomputers. Therefore, the electromagnetic problem has to be simplified and reduced.

3.3.1 Two-dimensional FDTD simulation

Good agreement between simulation and measurement results has indicated that the electromagnetic modelling based on the two-dimensional FDTD method is applicable for the hologram design. In the two-dimensional method, the hologram structure is assumed to be infinite and invariant in the vertical direction (y direction), as shown in Figure 3.4. When the electromagnetic behavior is studied in a narrow horizontal region (i.e., in a x cut), this is a fair approximation due to the gentle curvature of the slots and strips in the vertical direction. This approximation holds only for the holograms used to produce a plane wave.

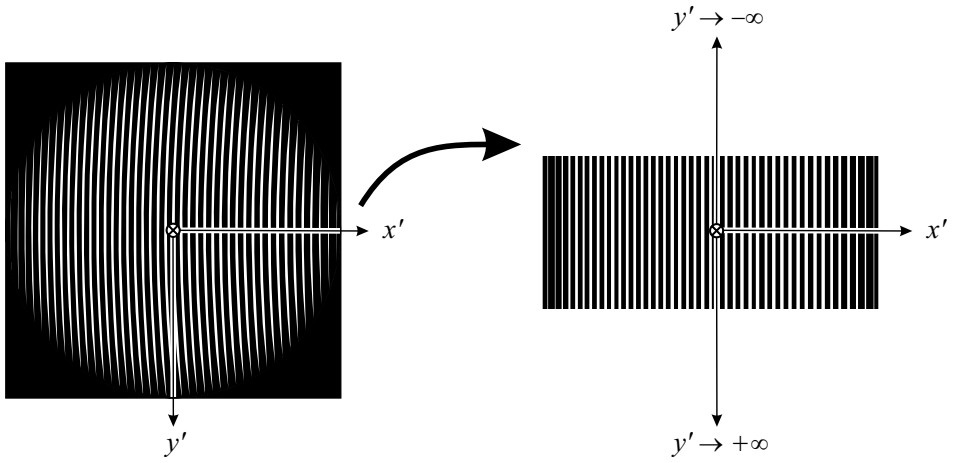

Figure 3.4: Simplification of a CATR hologram used in the FDTD simulation.

A scheme of the two-dimensional FDTD simulation is shown in Figure 3.5. The simulation domain is divided into rectangular cells: within each cell, local and time-dependent electric and magnetic fields are computed with Maxwell's equations using the central-difference approximations [97, 98]. The FDTD is a recursive method,

where the new field distributions are computed from the old ones at discrete times. The time step between computation rounds has to be small enough to make the simulation stable; the smaller the cell size is the shorter the time step has to be. The stability criteria are discussed in more detail in [98, 99].

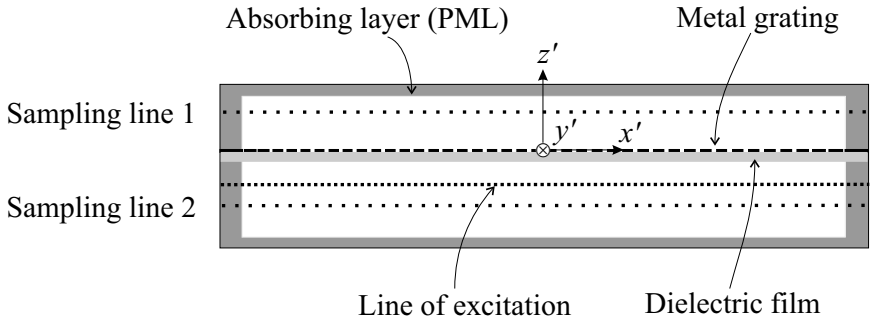

Figure 3.5: Two-dimensional FDTD simulation domain.

The cell size has to be kept small enough to model the hologram structure with a sufficient accuracy and to minimize the numerical dispersion. The numerical dispersion arises from the discretization of the simulation domain and causes variation of the numerical phase velocity with wave propagation angle [98]. The numerical phase velocity is always smaller than the physical phase velocity of the wave. If the cell dimensions are 0.1λ, the maximum phase velocity error relative to the physical phase velocity is –1.3 %, and it reduces to –0.3 % if the cell dimensions are 0.05λ [98].

A non-uniform grid is used to model the hologram structure accurately near the slot edges [100]. Smaller cells are used near the slot edges than elsewhere. The cells are gradually narrowed in the x direction towards the slot edges. By this way, the locations of the slot edges and the field in the vicinity of the edges are modelled more accurately. The use of larger cells further away from the slot edges helps to keep the computational size of the simulation reasonable. In the z direction, the cell width is fixed. The simulation domain is very wide in the x direction (up to hundreds of thousands of FDTD cells) but quite narrow along the z axis (approximately one hundred cells). The cell dimensions vary typically between 0.02–0.05λ, where λ is the wavelength in free space. If the wavelength is given in Mylar ($\epsilon_r = 3.35$) that is typically used as the hologram substrate, the variation of the cell dimensions is approximately 0.04–0.09λ.

In the two-dimensional FDTD simulation, two different polarizations are studied separately; the electric field is either parallel with the slots (y-directed) or perpendicular to them (tangential to the (x, z)-plane). The magnetic field is perpendicular to the electric field. In the first case (from now on called the vertical polarization), the electromagnetic field has components E_y, H_x, and H_z. In the latter case (the

horizontal polarization), the components are H_y, E_x, and E_z. Figure 3.6 shows the FDTD cells at the vertical and horizontal polarization. The cross-polarization analysis is not possible in the two-dimensional simulations, where the curvature of the slots, and thus the source of the cross polarization is omitted; a special method to analyze cross polarization is presented in [101].

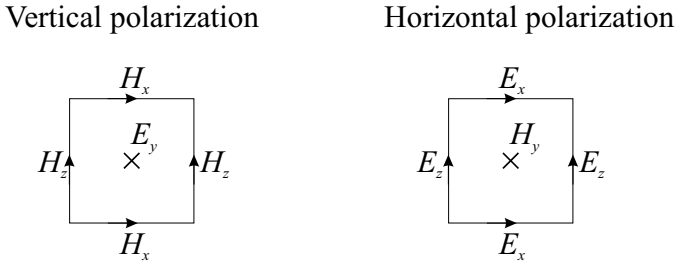

Figure 3.6: FDTD cells in the vertical and horizontal simulation.

The simulation domain is surrounded with an absorbing layer that serves to simulate the radiating free-space condition. The perfectly matched layer (PML) has been used for this purpose due to its very low reflectivity [98, 102].

3.3.2 Excitation

The sinusoidal excitation is placed a few cells away from the hologram structure (see Figure 3.5). The excitation is a so-called soft source, through which the reflected field can pass undisturbed [98]. At the line of excitation, the complex incident field is added to the computed field. At the vertical polarization, the incident electric field E_{in} is added to the electric field E_y. At the horizontal polarization, the equivalent incident magnetic field $H_{in} = E_{in}/\eta_0$ is added to the magnetic field H_y, which induces the electric field components E_x and E_z. The wave impedance of vacuum η_0 is 376.73 Ω.

Non-oscillating dc currents may be induced in the FDTD simulation, if the model has highly conductive current paths and the excitation is not turned on correctly [103, 104]. The hologram metal grating structure, which is modelled as a perfect electric conductor (PEC), is found to induce dc currents at the horizontal polarization. The dc-currents produce a stationary field, which can lead to interpretation errors in the post-processing of the simulation data. To avoid that, the dc-field components have to be filtered out from the simulation data. The filtering method has been used in earlier simulations. In this thesis work, however, an optimal ramp function has been used to turn the excitation smoothly on, which eliminates dc currents. It has

been found that a raised cosine function is optimal for this purpose [104]. When the excitation is turned on slowly during the first 4.5 sine wave cycles, no dc-field components can be observed in the simulation data.

3.3.3 Physical optics

The transmitted field in the aperture of the hologram is recorded along the sampling line (see Figure 3.5). In the post-processing, the time-domain data are transformed to the complex data, i.e., the amplitude and phase are resolved. From these data, the field further away from the hologram is calculated by using physical optics [63, 99]. The physical optics transformation is done on the same (x, z)-plane where the FDTD simulation is carried out.

In some simulations, the reflected field is the desired one [III,IV]. In such a case, the field in front of the hologram is recorded (see Figure 3.5). This is the total field including the reflected field and the field radiated from the excitation line towards the $-z$ axis. The reflected field can be determined by subtracting the excitation field from the total field. In this thesis work, the simulation method is extended in such a way that it can be used to calculate the reflected field, as well as the field over the full horizontal angle range [III,IV].

3.4 Manufacturing

The hologram pattern is processed on a thin dielectric film that serves as a mechanical support for the metal grating. For doing this, several different manufacturing methods have been investigated [9]. The hologram pattern can be manufactured either by using selective metal deposition or etching. In selective metal deposition, the dielectric film is placed in a liquid, where the metal layer is selectively grown to the film by using a laser. In etching, metal is selectively removed from the metal-plated dielectric film. This can be done either by using chemicals or by vaporizing metal with a laser. Some small holograms (200 mm in diameter) have been manufactured by using selective deposition or laser-vaporizing method, but chemical wet-etching has been found to be the most economical and the most convenient way to manufacture large holograms. Chemical wet-etching is commonly used in manufacturing of printed circuit boards (PCBs).

In etching process, the metal-plated dielectric film is first coated with photosensitive resist. Then, the pattern is exposed on the resist, and last the pattern is

chemically etched to the metal layer. Holograms smaller than 600 mm × 600 mm have been manufactured by using a photo mask to expose the pattern. According to experiments, photo masks can be used to manufacture holograms for frequencies up to 322 GHz [I]. However, laser exposure is found to be more suitable method to manufacture large holograms for high frequencies. In laser exposure, the hologram pattern is written directly to the photo resist with a computer-controlled laser. Since no photo mask is needed, manufacturing accuracy is improved. In the facility used currently for large holograms, the hologram film is placed on a cylinder [I]; by rotating the cylinder and moving the laser in the axial direction, the pattern is exposed on the film. The maximum area that can be processed with this facility is 1.2 m × 3.2 m and the nominal accuracy of the laser writing is 5 μm. According to the manufacturer, the manufacturing equipment can be modified quite easily to process patterns up to 1.5 m × 6 m in size.

A 50-μm-thick Mylar film laminated with a 17-μm-thick copper layer has been found to be electrically and mechanically a good substrate for holograms. The film has high-homogeneity and low permittivity, and also it is mechanically durable. According to the tabulated measurement data given at the frequencies of 140 GHz and 890 GHz in [105, 106], the relative permittivity of Mylar (polyethylene tetephthalate, PETP) is $\epsilon_r = 3.35$ at the ambient temperature of 300 K. A low permittivity is desirable to minimize the effect of the dielectric film on the propagation of the electromagnetic wave. The width of the 50-μm Mylar film currently available is 1.35 m. Also, a 25-μm-thick Mylar film with a 5-μm-thick copper plating has been used as a substrate material. This material is more suitable for higher frequencies ($\geq$650 GHz) than the 50 μm film, as the thinner dielectric film has a smaller disturbing effect on the operation of the hologram [VI]. The width of the 25 μm film currently available is approximately 1 m. As the skin depth of copper is very small at submillimeter wavelengths, even a thin copper layer blocks the transmission of the wave almost completely. For example, at 300 GHz, the skin depth of copper (with the conductivity of $\sigma_{Cu} = 5.8{\cdot}10^7$ S/m) is only [107]

$$\delta_{Cu} = 1/\sqrt{\pi f \mu_0 \sigma_{Cu}} = 0.12 \ \mu\text{m}. \tag{3.6}$$

As the maximum area that can be processed in a single piece is 1.2 m × 3.2 m, large holograms up to several meters in diameter have to be made in several pieces. To avoid discontinuities in the hologram pattern, the pieces have to be aligned carefully and joined together by using a method that does not disturb propagation of the electromagnetic wave. Taping, gluing, and soldering have been tested as potential methods to join the hologram pieces together [9], [I]. At submillimeter wavelengths, taping and gluing increase the electrical thickness of the substrate significantly, which causes distortions to the quiet-zone field. In the soldering method, the horizontal hologram pieces are joined together by soldering the vertical metal strips

together [I]. According to experiments, a soldered seam is mechanically durable and it does not disturb the electromagnetic wave, i.e., it is electrically almost invisible, if the pieces are aligned accurately.

3.5 Properties of the hologram as a collimator

If the hologram is used as a transmission-type element, the rms surface planarity requirement is approximately 0.1λ, which is moderated by a factor of ten from the planarity requirement of a reflector (0.01λ) [108]. A moderated planarity requirement is a significant advantage at submillimeter wavelengths, where manufacturing tolerances become extremely tight. According to several experiments, sufficient planarity is achieved by tensioning the hologram to a frame. The rms manufacturing accuracy requirement of the hologram pattern is approximately 0.01–0.02λ [99].

Because the hologram is a diffractive element, it is bandlimited. The relative band width of the hologram is estimated to be ±5–10 % [63]. The narrow band width is not a serious disadvantage as the antenna tests are usually done at discrete frequencies and the low manufacturing cost permits to make separate holograms for the different frequencies needed.

If the hologram is illuminated with a horn antenna, it can be designed to work optimally only at the vertical polarization [63, 100]. This is because the amplitude modification required to compensate the Gaussian illumination can be realized reasonably only at the vertical polarization. The curvature of the slots depolarize the diffracted field. The curvature of the slots can be reduced by placing the feed further away from the hologram, which reduces cross-polarization. As the hologram pattern is symmetric with respect to its horizontal centerline, cross-polarization at the horizontal centerline of the quiet-zone is very low (in theory, it is zero). Cross-polarization rises towards the edges of the quiet-zone and is typically up to –15 to –20 dB for the holograms illuminated with a horn [28, 101]. The polarization characteristics of the hologram can be improved significantly by using a shaped illumination produced with a dual reflector feed system (DRFS). This is discussed more in Chapter 5.

Due to partial blocking of the incident field, the transmission loss of the binary amplitude hologram is rather high. In addition, only a portion of the transmitted power propagates to the quiet-zone; the rest is diffracted to other directions [III]. According to the measurements done in [IV], the total power loss of a transmission-type hologram is 11.4 dB, when the quiet-zone field amplitude is compared to the hologram illumination. The power loss reduces the dynamic range available in mea-

surements. Therefore, in RCS measurements, where a very high dynamic range is required, the use of a binary amplitude hologram is not practical. Instead, a phase hologram has been used in these measurements due to its much lower power loss that is approximately 4 dB [96].

For a circular hologram, the quiet-zone is approximately 50–65 % of the diameter of the hologram in the horizontal direction and 60–77 % in the vertical direction. In the horizontal direction, the oblique propagation angle (33°) narrows the quiet-zone. If the feed is a horn, the quiet-zone is limited by the edge tapering of slots, which has to be sufficient to eliminate edge diffraction. Instead, if the DRFS is used as the feed, the quiet-zone is limited by the –1-dB beam width of the illumination. Typically, the relative size of the quiet-zone increases, when the electrical size of the hologram is increased.

4 Hologram-based compact antenna test range at submillimeter wavelengths

The hologram-based CATR has earlier been used successfully for antenna tests at millimeter wavelengths [64, 65, 93]. After that, the research work has focused on upgrading the hologram-based CATR for the submillimeter-wave range to respond to increasing demand for antenna tests at this range. The research work carried out has been presented in [I–VI] and is discussed here briefly.

4.1 Hologram-based CATR at 322 GHz

In 2003, the development work culminated in construction of a hologram-based CATR for 322 GHz [I]. The hologram was 3 m in diameter and made from three pieces. For demonstration, the Admirals RTO [82], a 1.5 m reflector antenna, was tested in this CATR [II]. The Admirals RTO had already been tested in a reflector-based CATR at 322 GHz [82] so it was most natural to carry out the antenna tests in the hologram-based CATR at the same frequency. The work was carried out successfully, showing the hologram-based CATR to be feasible also for submillimeter-wave antenna testing.

Design and construction of the CATR, as well as the electrical verification tests are presented in [I]. The CATR was constructed in a large hall at TKK, which is not originally intended for antenna testing (see Figure 4.1). However, by designing the range layout carefully and by using absorbers in appropriate places to eliminate reflections, it was possible to modify the hall to be suitable for antenna testing. The assembly of the range, the antenna tests, and finally the disassembly were all done in about two months. This shows that the hologram-based CATR can really be used as a temporary and transportable antenna test facility.

In construction of the CATR, the major concern related to the design and manufacturing of the hologram. Finding a commercial facility that can process large patterns with a sufficient accuracy was a challenging task. The facility based on chemical wet-etching and laser-exposure (see Section 3.4) was found to be the most suitable method for this purpose. The hologram was manufactured in three horizontal pieces, each 1 m $\times$ 3 m in size, which were joined together by soldering. A vacuum table and special equipment were developed to align, cut, and solder the pieces. Everything was tested first with 1:5 scale models (600 mm holograms operating at 322 GHz) to see if any problems arise in the design, manufacturing,

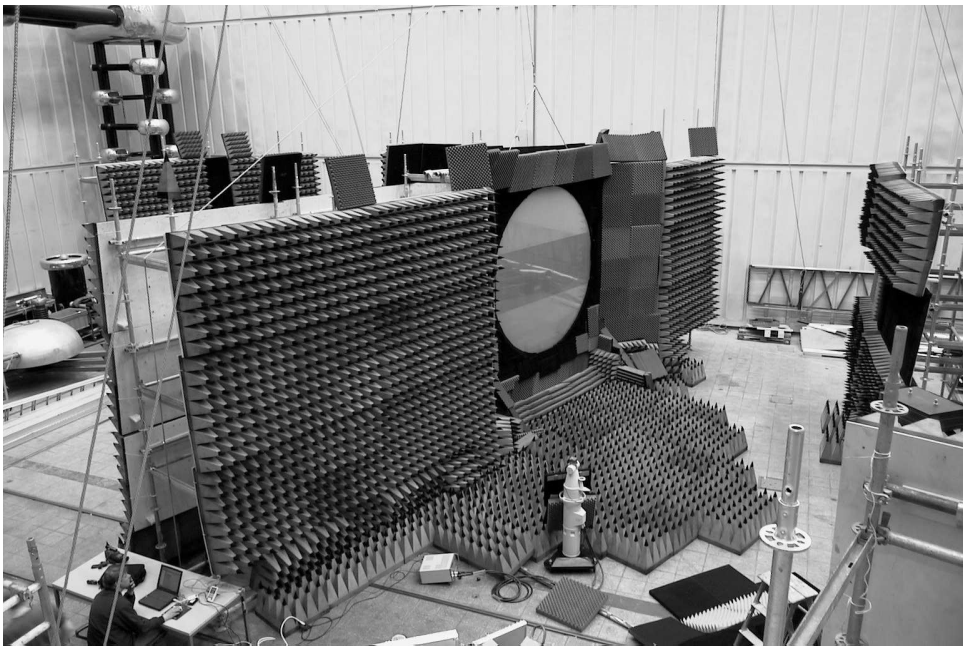

Figure 4.1: Photograph of the CATR. The feed is located in the top left corner, the hologram is seen in the middle, and the AUT is placed in the bottom right corner.

or construction of the hologram. The quiet-zone of the scale model holograms was also tested. The same substrate material (50 μm Mylar film) was used for the scale models as for the 3 m hologram. In addition, the slot and strip widths were approximately the same for the scale models as for the 3 m hologram. The geometries and dimensions of the CATRs were also the same, except in 1:5 scale. In this way, it was more likely to detect and eliminate all possible problems that could appear in the 3 m hologram.

The simulated quiet-zone amplitude and phase ripples of the 3 m hologram were less than 0.5 dB and 5°, peak-to-peak. The width of the simulated quiet-zone was 1.95 m in the horizontal direction, which was estimated to be very sufficient for the 1.5 m Admirals RTO. As the corrugated horn was used for illumination, the hologram was designed to operate at the vertical polarization only. The simulation results are presented in [5, 7, 11].

The quiet-zone of the 3 m hologram was measured with a plane-polar scanner in the horizontal, vertical, and diagonal directions. A corrugated horn, having a gain of approximately 20 dB, was used as the probe. The electrical instrumentation was based on the AB Millimètre MVNA-8-350 vector network analyzer making possible also the phase measurements. The dynamic range was about 52 dB, which was

considered to be sufficient to give accurate amplitude and phase measurement results. The measured quiet-zone amplitude and phase deviations were 2.6 dB and 250°, peak-to-peak, within an area of 1.5 m in diameter covering the aperture of the Admirals RTO. Two features were clearly observed in the quiet-zone field: an amplitude dip of 1–1.2 dB towards the center of the quiet-zone and a 250° saddle-shaped equiphase surface.

After the quiet-zone testing, the scanner was removed and the Admirals RTO was mounted on the antenna positioner. The antenna measurements were done by using a spectrum analyzer and the receiver unit supplied with the Admirals RTO. As the Admirals RTO has a gain (approximately 70 dB at 322 GHz [82]) much higher than that of the corrugated horn, the dynamic range was increased to 85 dB in the antenna measurements. However, due to a lower receiver sensitivity in this setup, the increase of the dynamic range was only approximately 33 dB, not 50 dB, as one could have expected on the basis of the difference in gains of the antennas.

The horizontal and vertical cut of the antenna pattern were measured: the angle range was ±85° in the horizontal direction and ±12° in the vertical direction. In addition, a two dimensional scan was done over the main beam region. The measured –3-dB beam width was 0.050° in the horizontal cut and 0.086° in the vertical cut. The corresponding simulated beam widths were 0.045° and 0.053°.

4.1.1 Non-idealities in the CATR and their effect

Distortions in the quiet-zone field and their effect on the antenna measurement results were analyzed. Apparently, the amplitude dip was partially caused by slightly inaccurate modelling of the hologram in FDTD. As the hologram was very large, the FDTD cell width was increased in the x direction to keep the simulation size and time tolerable. When the hologram was later simulated with a denser grid, an amplitude dip of 0.5 dB appeared in the quiet-zone field. Therefore, during the design, the hologram was perhaps modelled with a too coarse FDTD grid.

According to microscope measurements, manufacturing accuracy of the hologram pattern was good: the average manufacturing error in the slot widths was only 10 μm and no systematic error was observed. However, the measurement uncertainty of the microscope measurements was rather large; it was estimated to be ±15 μm. It has been noticed that systematically too narrow slots produce an amplitude dip in the quiet-zone field, if the hologram pattern is designed for the horn illumination (for example, see quiet-zone simulation results in [VII]). Within the measurement uncertainty, it may have been possible that the slots in the manufactured hologram pattern were systematically 15 μm narrower than the ideal slots. According to

simulations done afterwards, this kind of manufacturing error produces an amplitude dip of 0.6 dB in the quiet-zone field. Thus, within the measurement uncertainty, a part of the measured amplitude dip may have been due to a slight systematic manufacturing error.

Most likely, due to an error in the manufacturing process, the hologram pattern was deformed slightly so that its width was 3000 mm and height 2990 mm. Simulations done for this kind of pattern suggest that the 250° saddle-shape phase deviation in the quiet-zone field was mainly caused by this deformation. Perhaps, due to this deformation, alignment of the hologram pieces was difficult on the pattern edges, and therefore the alignment error perpendicular to the seams was up to 1 mm. This can explain partly large phase deviations measured on the edges of the quiet-zone.

As the imperfections in the quiet-zone field were rather large, it was necessary to estimate their effect on the measured antenna radiation pattern. For example, systematical quiet-zone distortions shape the measured main beam, change its width, and change the magnitude of the side lobes. In addition, amplitude and phase ripples in the quiet-zone field and reflection from the surroundings may produce extraneous side lobes. After an extensive analysis carried out in [II], it was possible to estimate the effect of the CATR imperfections reasonably well and to give a qualitatively evaluation of the actual operation of the Admirals RTO.

4.2 Hologram as a reflection-type collimator at 310 GHz

In Publication [III], holograms were studied more widely as a quasi-optical element for shaping radio-wave fields. For this purpose, the radiation pattern of a binary amplitude hologram was simulated over the full horizontal angle range to show for the first time all the beams diffracted from the hologram. According to this simulation result, a transmission-type hologram also reflects a plane-wave, which can be several decibels higher than the transmitted one.

In Publication [IV], feasibility of the binary amplitude hologram as a reflection-type element was studied more closely. The hologram was 600 mm in diameter and designed to operate at 310 GHz in a transmission-type setup. According to simulation results, the amplitude and phase ripples were slightly larger in the reflected plane wave than in the transmitted one. This was partly due to the fact that the pattern was not optimized for the reflection-type operation. In the reflection-type setup, the operation of the hologram is based on the reflection from the metal strips, and therefore the metal strip widths should be tuned to produce an optimal reflection; not the slot widths to produce an optimal transmission, as it was done in this hologram.

The transmitted and reflected plane waves were also measured. The measurements were done with the MVNA and a planar scanner. In the reflection-type setup, the location of the feed was a mirror image to that of the transmission-type setup. To eliminate the transmitted field, an absorber wall was placed behind the hologram in the reflection-type setup. In the transmitted plane wave, the measured peak-to-peak ripples were 1.2 dB and 10°, and in the reflected plane wave, they were 1.6 dB and 20°. The phase of the reflected plane wave was slightly convex, apparently, due to a small misalignment of the feed. The amplitude level was approximately 4 dB higher for the reflected plane wave than for the transmitted one. This was quite obvious, as the metal strips in this hologram were at least three times wider than the slots making the reflected field much higher than the transmitted one. The power loss was also measured: the quiet-zone amplitude level was compared to the maximum amplitude level of the horn illumination in the hologram aperture. By this way, it was calculated that the power loss was approximately 11.4 dB in the transmission-type setup and 7.4 dB in the reflection-type setup.

The reflection-type setup was also used to measure the radiation pattern of a small lens-type antenna [109]. The radiation pattern measured in the reflection-type setup agreed well with the one measured in the transmission-type setup. This indicates that also the reflection-type hologram is suitable for antenna testing. According to these experiments done at 310 GHz, the planarity achieved by tensioning the hologram on a frame is sufficient even for the reflection-type operation.

4.3 Hologram-based CATR at 650 GHz

In future, antenna tests may be needed at even higher frequencies. Therefore, it was investigated whether it is possible to build a hologram-based CATR for higher submillimeter-wave frequencies. In Publication [V], a hologram of 300 mm in diameter was designed for 650 GHz and its quiet-zone was tested. The hologram was manufactured on the 25 μm Mylar film. In Publication [VI], two holograms approximately 1 m in diameter were tested at 644 GHz. One of these holograms was manufactured on the 25 μm Mylar film and the other on the 50 μm film.

It was noticed that, if the dielectric film is electrically too thick, the field inside the film starts to resonate, which ruins the quiet-zone field. According to simulations carried out in [VI], the 50 μm Mylar film can be used as the substrate at frequencies up to 650 GHz, if the hologram is designed properly to eliminate resonances. It has been estimated that the 25 μm Mylar film could be suitable for frequencies up to 1000 GHz [VI].

Chemical wet-etching with laser exposure was used to manufacture the holograms. Manufacturing accuracy was inspected with a camera microscope. Excluding the systematic manufacturing error, the random manufacturing error in the slot widths was measured to be only ± 5 μm in the hologram manufactured on the 50 μm Mylar film. Assuming the random error to be uniformly distributed, the rms random manufacturing error was approximately 2.9 μm that is 0.006λ at 650 GHz. At 1000 GHz, the rms random manufacturing error would be 0.01λ. The systematic manufacturing error (i.e., slots being too wide) was approximately 20 μm. It may be possible to reduce the systematic manufacturing error significantly by calibrating the manufacturing process more carefully. After that, the manufacturing method should be accurate enough for holograms operating at frequencies up to 650 GHz, or even up to 1000 GHz.

The research work at 650 GHz has been continued. In autumn 2006, the Admirals RTO was measured in a hologram-based CATR at 650 GHz [30, 32]. The 650 GHz CATR was very similar to the one presented in [I]. However, a dual reflector feed system (DRFS) was used for illumination in this setup. The hologram was 3.16 m in diameter and was made of three pieces by soldering them together as in [I]. The work was carried out successfully and the results are currently being analyzed.

5 Improved characteristics of the hologram by using a dual reflector feed system

In this chapter, the dual reflector feed system (DRFS) is introduced and its use for illumination of holograms is considered. In Publications [VII–IX], it has been demonstrated by simulations and experiments, how characteristics of the hologram can be improved by using the DRFS for illumination.

5.1 Dual reflector feed system

A dual reflector feed system is used to produce a shaped illumination that is flat in the middle of the hologram and strongly tapered towards the edges. When the hologram is designed for the DRFS illumination, amplitude modification is not needed, and therefore the slots can be almost uniform in width; the hologram is only used to transform the spherical phase front to a planar one. Compared to a conventional hologram pattern designed for a horn illumination, the DRFS hologram pattern has several advantages related to its electrical characteristics and manufacturing properties. In addition, as the DRFS concentrates the radiation on the hologram, the spill over radiation is decreased, which improves power efficiency and reduces reflections from the hologram edges and surroundings. Figure 5.1 shows the prototype DRFS constructed for 310 GHz [110]. The DRFS consists of two shaped reflectors and produces a 5-th order Butterworth-type beam.

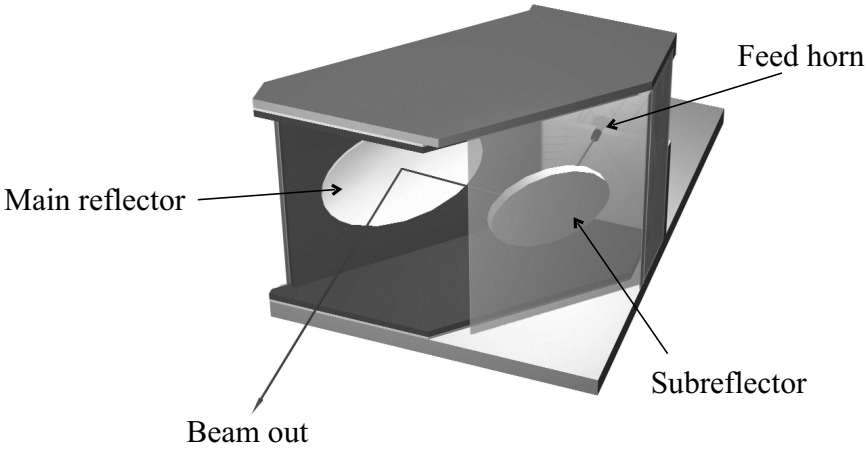

Figure 5.1: Artistic view of the 310 GHz DRFS.

According to measurements, the actual DRFS beam differs only slightly from the ideal one [VII]. This is desirable, because the ripples in the DRFS beam increase directly the overall ripples in the quiet-zone field. The DRFS is designed to illuminate holograms of 600 mm in diameter from a 1.8 m distance; the –1 dB beam width of the illumination is 370 mm and the edge illumination is approximately –15 dB. The DRFS can be used for holograms of different size as well, as long as the relative focal distance remains approximately the same.

5.2 Improved manufacturing properties

In Publication [VII], two 600 mm holograms were designed for 310 GHz: one hologram was designed for a corrugated feed horn, the other for the DRFS. Both holograms were optimized for the vertical polarization. According to measurements, the holograms operated reasonably well and their quiet-zone ripples were approximately of the same order of magnitude. The manufacturing accuracy was approximately the same for both holograms.

Systematic manufacturing errors (i.e., slots are systematically narrower or wider than designed) are common in etching processes. A systematic error in slot widths causes mainly amplitude distortions in the quiet-zone field; its effect on the phase is usually small. In [VII], it was studied by simulations, what is the maximum systematic manufacturing error still acceptable to keep the quiet-zone amplitude deviations within 1 dB, peak-to-peak. It was noticed that in the DRFS hologram the slots can be up to 100 μm too wide without significant degradation of the quiet-zone amplitude, whereas in the hologram illuminated with a horn the slots can be 30 μm too wide at maximum.

When a horn is used for illumination, slots have to be narrowed towards the edges of the hologram to eliminate edge diffraction. It has been noticed that narrow slots are difficult to etch properly, which may increase edge diffraction. For example, see the manufacturing results of Hologram II in [VI], where the narrow slots are not completely etched, which reduces the diameter of the pattern and increases edge diffraction. Manufacturing becomes easier, if the narrow slots can be avoided as in the DRFS hologram.

5.3 Operation at the horizontal polarization

In Publication [VIII], operation of the DRFS hologram was studied at the horizontal polarization. The quiet-zone of the DRFS hologram presented in [VII] was simulated and measured at the horizontal polarization. Although this hologram was designed to operate at the vertical polarization only, it operates reasonably well also at the horizontal polarization.

Encouraged by these results, it was studied whether a hologram illuminated with the DRFS could be optimized for the horizontal polarization. According to preliminary simulation results presented in [VIII], a DRFS hologram can be optimized for the horizontal polarization so that it operates fairly well at the vertical polarization as well. However, its operation at different polarizations is not identical, but the amplitude level is approximately 4 dB lower at the horizontal polarization than at the vertical polarization.

5.4 Operation at the circular polarization

Operation of a DRFS hologram at different polarizations was studied further in Publication [IX]. The purpose was to design a hologram for 310 GHz, which operates identically at the horizontal and vertical polarization. Such a hologram could be used for measurements of circularly polarized antennas.

The hologram design was started by studying transmission of a hologram slot structure more closely at 310 GHz. It was noticed that transmissions at the horizontal and vertical polarization coincide, if slots are very wide, i.e., $>0.6\lambda$. At small slot widths, transmissions at different polarizations diverge significantly. If slots are narrower than $<0.4\lambda$, transmission at the vertical polarization depends strongly on the slot width, which makes amplitude tuning possible. At the horizontal polarization, transmission does not depend so strongly on the slot width, and thus amplitude tuning is difficult to realize (it would require a very large variation of slot widths). When the hologram is designed for the vertically polarized horn illumination, the slots are usually less than 0.4λ in width.

Two holograms were designed for 310 GHz. Their operation at different polarizations was optimized to be as identical as possible. One hologram was designed for the 25 μm Mylar film, the other for the 50 μm Mylar film. It was noticed that optimization was slightly more difficult with the 50 μm Mylar film, as the thicker dielectric film has a stronger disturbing effect on the operation of the hologram. However,

according to simulations, both holograms operate very well and the quiet-zone field is almost independent of the polarization.

5.5 Reduced cross polarization

The curvature of the slot depolarizes the transmitted field. However, if the transmissions at the polarizations parallel and perpendicular to the slot are close to each other, the depolarization effect is low [101]. At large slot widths the transmissions at different polarizations coincide [IX], which reduces cross-polarization. Cross-polarization level of a hologram illuminated with a horn antenna is rather high (–15 to –20 dB) due to narrow slots on the pattern edge used to eliminate edge diffraction [28, 101].

Cross polarization of the holograms in [IX] was simulated by using the method presented in [101]. According to simulations, cross-polarization pattern for both holograms is very similar at different polarizations. The maxima locates on the edge of the quiet-zone where the cross-polarization level is approximately –26 dB, i.e., it is 6–11 dB lower than that of a hologram designed for the horn illumination. The overall cross polarization of the CATR is a result of the cross polarization produced by the feed and the hologram. The cross-polarization of a corrugated horn is typically low, approximately –40 dB, and thus its effect on the overall cross-polarization is negligible. According to measurements, the cross-polarization of the DRFS is rather high, approximately –23 dB [111], which may increase the overall cross-polarization of the CATR unless reduced. In future, it might be necessary to optimize also the cross-polarization performance of the DRFS.

6 Summary of publications

Publication [I] presents the hologram-based compact antenna test range (CATR) constructed for 322 GHz. For the first time, the hologram-based CATR has been used for submillimeter-wave antenna tests. In the publication, design and construction of the CATR are described including the measurement instrumentation and the 3 m hologram that was joined from three pieces by soldering. Also, the quiet-zone measurement results are presented and distortions observed in the quiet-zone field are analyzed.

Publication [II] presents the antenna tests done for the Admirals RTO in the CATR introduced in [I]. The measured antenna radiation patterns are shown and they are compared to the simulated ones. The effect of the quiet-zone distortions is evaluated by simulations.

Publication [III] discusses different types of radio-wave holograms and applications they can be used for. In addition, the hologram design methods are briefly discussed and some measurement results are shown. For the first time, the simulated radiation pattern of a CATR hologram is presented over the full horizontal angle range. The simulation done at 650 GHz for a 1 m hologram shows all the beams radiated from the hologram including the reflected ones.

Publication [IV] considers the possibility to use hologram as a reflection-type collimator. Simulations and measurements done at 310 GHz show that a transmission-type binary amplitude hologram also reflects a high-quality plane wave. Demonstrative antenna measurements show that the reflection-type hologram is suitable for actual antenna testing. In addition, the power loss of the hologram was measured. According to measurement, the power loss in the reflection-type setup is approximately 7.4 dB that is 4 dB lower than that in the transmission-type setup.

Publication [V] takes the first steps towards the hologram-based CATR at 650 GHz. Simulation and measurement results of a small (300 mm diameter) hologram are presented. The results are promising and encouraging for further study.

Publication [VI] continues the research at 650 GHz. Two 1 m holograms are designed, manufactured and tested. It is observed that the quiet-zone field is distorted, if the hologram substrate is electrically too thick. The 50-μm-thick Mylar film is found to be suitable for frequencies up to 650 GHz and the 25-μm-thick Mylar film is estimated to be suitable even for 1000 GHz. Reasonably good measurement results suggest that the hologram-based CATR is potential for 650 GHz, even for 1000 GHz.

Publication [VII] discusses the dual reflector feed system (DRFS) and its use for illumination of holograms. The DRFS illumination allows to use a simplified hologram pattern, which is more robust for manufacturing errors.

Publication [VIII] considers the possibility to design a hologram that operates at the horizontal polarization; previously, when a horn antenna has been used for illumination, operation has been limited to the vertical polarization. Measurements and simulations done at 310 GHz suggest that operation at the horizontal polarization is possible if the DRFS is used for illumination. It seems possible to design a hologram that operates both at the horizontal and vertical polarizations at the same time.

Publication [IX] continues the research started in [VIII]. Here, the goal has been to design a hologram that operates identically at the vertical and horizontal polarization so that it could be used for measurements at the circular polarization. Transmission of a hologram structure is studied. It is observed that transmissions at different polarizations coincide at very large slot widths, i.e., when the slots and strips are approximately equal in width. Two holograms have been designed for 310 GHz. According to simulation results, the quiet-zone fields at different polarizations are almost identical. It is also observed that large slots reduce cross polarization significantly.

7 Conclusions and research in future

The hologram-based compact antenna test range (CATR) has shown its capability at submillimeter wavelengths. A CATR based on a 3 m hologram was constructed for testing a 1.5 m reflector antenna at 322 GHz [I,II]. All this work, including the antenna tests and the disassembly of the CATR, took only two months, and thus showed that the hologram-based CATR can really be used as a transportable, temporary antenna test facility. Mainly due to difficulties in the hologram manufacturing, amplitude and phase deviations in the quiet-zone field were larger than expected. However, by careful analysis, it was possible to estimate their effect on the measured antenna radiation pattern and evaluate the actual operation of the antenna.

Capability of the hologram-based CATR was also demonstrated at 650 GHz [V,VI]. In [VI], two 1 m holograms were manufactured on different substrates and they were tested. It was found that the 50 μm Mylar film can be used as the substrate for holograms operating at frequencies up to 650 GHz. At higher frequencies, the film has to be thinner to avoid resonances inside the film. The other hologram was manufactured on the 25 μm Mylar film, which is estimated to be suitable up to 1000 GHz.

Direct laser-exposure combined with chemical wet-etching has proven to be sufficiently accurate method up to 650 GHz, and possibly after more careful calibration it could be used even at 1000 GHz. This method is capable to process patterns that are at maximum 1.2 m $\times$ 3.2 m in size. According to the manufacturer, the manufacturing equipment can be modified quite easily to process patterns up to 1.5 m $\times$ 6 m in size. The 3 m hologram in [I] was made from three pieces by soldering the pieces together. Soldering has been found to be an excellent joining method, as the soldered seam does not cause distortions, as long as the pieces are aligned accurately.

Unfortunately, alignment of the pieces has turned out to be very challenging. Thus, manufacturing of high-quality submillimeter-wave holograms (fulfilling the 1 dB/10° quiet-zone planarity requirement) seems to be possible only, if the pattern is manufactured in one piece. Using the 50 μm Mylar film that is 1.35 m wide, it should be possible to design a hologram, which produces a quiet-zone of approximately 1 m in diameter. This requires that the hologram pattern is elliptical so that the quiet-zone is circular in shape. Such a hologram could be used for testing an antenna approximately 0.8–0.9 m in diameter. Using the 25 μm Mylar film that is 1 m wide, a 0.7 m quiet-zone should be possible, and thus the maximum antenna size could be 0.5–0.6 m. It appears that the hologram-based CATR could be used for testing

approximately a half meter antenna even at 1000 GHz.

The possibility was also studied to use the binary amplitude hologram as a reflection type element [III,IV]. Quiet-zone simulations and measurements, as well as antenna tests done at 310 GHz have showed that a transmission-type hologram can also be used as a reflection-type element. According to these experiments, it seems that the planarity achieved by tensioning the hologram on a frame is sufficient even for the reflection-type operation. Advantages of the reflection-type hologram are the more compact setup and higher power efficiency. The performance of the hologram should be optimized for the reflection-type operation. In addition, it should be studied whether the reflection-type hologram could have some advantages related to its manufacturing. As the operation of the reflection-type hologram is essentially based on reflection from the metal strips, the substrate behind the strips has presumably a smaller effect on the operation than it would be in the transmission-type setup. At frequencies above 1000 GHz the substrate material has to be very thin ($<$25 μm) to avoid resonances in the transmission-type hologram. In the reflection-type hologram, it could be possible to use a thicker substrate, which would be a great advantage at high frequencies. It could be possible even to manufacture the hologram metal grating on a thick self-standing panel made of low-permittivity dielectric material. Large holograms could be made from several panels. Due to the self-standing structure of panels, joining of panels could be relatively easy. The reflection-type hologram seems to be a reasonable alternative to a conventional shaped reflector due to its planar structure, which can be manufactured relatively simply by using the PCB manufacturing technique.

Properties of the hologram can be improved significantly by using a simplified hologram pattern, which only transforms the spherical phase front to planar one; the amplitude is modified with a dual reflector feed system (DRFS). Slots in the simplified hologram pattern are almost uniform in width and they can be much wider than in the conventional hologram pattern designed for a horn illumination. This facilitates manufacturing, reduces cross polarization, and makes operation at the horizontal polarization possible [VII,VIII]. The hologram pattern can be designed so that its operation does not depend on the polarization [IX], i.e., it can also be used at the circular polarization. Such a hologram has been designed for 310 GHz and is going to be tested soon.

In autumn 2006, the Admirals RTO was measured in a hologram-based CATR at 650 GHz [30, 32]. The 650 GHz CATR was very similar to the one presented in [I]. However, a DRFS was used for illumination in this setup. The hologram was 3.16 m in diameter and was made of three pieces by soldering them together as in [I]. The work was carried out successfully and the results are currently being analyzed.

References

[1] A. V. Räisänen, J. Ala-Laurinaho, J. Säily, J. Häkli, T. Koskinen, A. Lönnqvist, and J. Tuovinen, "Radio hologram CATR – a feasible method for FIRST/Herschel Space Observatory antenna testing?" in *Proc. Submillimeter Astronomy Science Workshop for Far Infrared Submillimeter Telescope (FIRST)*, San Diego, CA, Feb. 2001, CD-ROM.

[2] J. Häkli, J. Säily, J. Ala-Laurinaho, T. Koskinen, A. Lönnqvist, A. Lehto, J. Tuovinen, and A. V. Räisänen, "Development of a hologram CATR for submm-wavelengths," in *Proc. 12th International Symposium on Space Terahertz Technology*, San Diego, CA, Feb. 2001, pp. 390–399.

[3] A. V. Räisänen, J. Ala-Laurinaho, J. Säily, J. Häkli, T. Koskinen, A. Lönnqvist, V. Viikari, J. Mallat, E. Noponen, J. Salo, J. Meltaus, M. Weber, and M. M. Salomaa, "Computer generated holograms for mm- and submm-wave applications: CATR, bessel beams and radiowave vortices (invited paper)," in *Proc. 9th International Conference on Terahertz Electronics*, Charlottesville, VA, Oct. 2001, CD-ROM.

[4] A. V. Räisänen, J. Ala-Laurinaho, J. Säily, J. Häkli, T. Koskinen, A. Lönnqvist, E. Noponen, J. Salo, J. Meltaus, J. Westerholm, and M. M. Salomaa, "Experimental studies on radio holograms at mm- and submm-wavelengths (invited paper)," in *MSMW'01 Symposium Proceedings, The Fourth International Kharkov Symposium on Physics and Engineering of Millimeter and Submillimeter Waves*, Kharkov, Ukraine, June 2001, pp. 57–62.

[5] J. Säily, J. Ala-Laurinaho, J. Häkli, T. Koskinen, A. Lönnqvist, J. Tuovinen, and A. V. Räisänen, "Measuring satellite antennas with a compact hologram test range," *IEEE Aerospace and Electronic Systems Magazine*, vol. 17, no. 5, pp. 13–19, May 2002.

[6] J. Meltaus, J. Salo, E. Noponen, M. M. Salomaa, A. Lönnqvist, T. Koskinen, J. Säily, J. Häkli, J. Ala-Laurinaho, J. Mallat, and A. V. Räisänen, "Holograms for shaping radio-wave fields," in *Proc. IEEE MTT-S International Microwave Symposium*, Seattle, WA, June 2002, pp. 1305–1308.

[7] T. Koskinen, J. Ala-Laurinaho, J. Säily, J. Häkli, A. Lönnqvist, J. Mallat, J. Tuovinen, and A. V. Räisänen, "On the design of sub-mm wave amplitude holograms for CATR," in *Proc. 13th International Symposium on Space Terahertz Technology*, Cambridge, MA, Mar. 2002, pp. 537–543.

[8] J. Häkli, T. Koskinen, J. Ala-Laurinaho, J. Säily, A. Lönnqvist, J. Mallat, J. Tuovinen, and A. V. Räisänen, "A dual reflector feed system for a sub-mm hologram CATR," in *Proc. 13th International Symposium on Space Terahertz Technology*, Cambridge, MA, Mar. 2002, pp. 327–336.

[9] A. Lönnqvist, J. Ala-Laurinaho, J. Häkli, T. Koskinen, V. Viikari, J. Säily, J. Mallat, J. Tuovinen, and A. V. Räisänen, "Manufacturing of large-sized amplitude holograms for a submm-wave CATR," in *Digest of 2002 IEEE Antennas and Propagation Society International Symposium*, vol. 4, San Antonio, TX, June 2002, pp. 394–397.

[10] J. Häkli, J. Ala-Laurinaho, T. Koskinen, J. Säily, A. Lönnqvist, J. Mallat, J. Tuovinen, and A. V. Räisänen, "Synthesis of a dual reflector feed system for a hologram CATR," in *Digest of 2002 IEEE Antennas and Propagation Society International Symposium*, vol. 4, San Antonio, TX, June 2002, pp. 580–583.

[11] T. Koskinen, J. Häkli, J. Säily, A. Lönnqvist, J. Ala-Laurinaho, J. Mallat, J. Tuovinen, A. V. Räisänen, and J. Lemanczyk, "Hologram CATRs for 322 and 650 GHz: a progress report," in *Proc. 25th ESA Antenna Workshop on Satellite Antenna Technology*, ESTEC, Noordwijk, The Netherlands, Sept. 2002, pp. 165–171.

[12] A. V. Räisänen, J. Meltaus, J. Salo, T. Koskinen, A. Lönnqvist, J. Häkli, J. Säily, J. Ala-Laurinaho, J. Mallat, E. Noponen, and M. M. Salomaa, "Computer-generated holograms for mm- and submm-wave beam shaping (invited paper)," in *Conference Digest of the 27th IEEE International Conference on Infrared and Millimeter Waves IRMMW2002*, San Diego, CA, 2002, pp. 113–114.

[13] J. Meltaus, J. Salo, E. Noponen, M. M. Salomaa, V. Viikari, A. Lönnqvist, T. Koskinen, J. Säily, J. Häkli, J. Ala-Laurinaho, J. Mallat, and A. V. Räisänen, "Millimeter-wave beam shaping using holograms," *IEEE Transactions on Microwave Theory and Techniques*, vol. 51, no. 4, pp. 1274–1280, Apr. 2003.

[14] J. Häkli, T. Koskinen, A. Lönnqvist, J. Ala-Laurinaho, J. Mallat, J. Säily, J. Tuovinen, A. V. Räisänen, and J. Lemanczyk, "Dual reflector feed system for sub-mm wave region hologram CATR," in *Proc. 3rd ESA Workshop on Millimetre Wave Technology and Applications*, Espoo, Finland, May 2003, pp. 353–358.

[15] J. Ala-Laurinaho, J. Säily, T. Koskinen, J. Häkli, A. Lönnqvist, J. Mallat, J. Tuovinen, and A. V. Räisänen, "Preparations for testing the ADMIRALS RTO in an ad hoc CATR based on a hologram," in *Proc. 3rd ESA Workshop on Millimetre Wave Technology and Applications*, Espoo, Finland, May 2003, pp. 389–394.

[16] J. Häkli, J. Mallat, J. Säily, J. Ala-Laurinaho, A. Lönnqvist, T. Koskinen, and A. V. Räisänen, "Improving the measurement accuracy of a planar near-field scanner for submillimetre wave antenna testing," in *Proc. 3rd ESA Workshop*

on Millimetre Wave Technology and Applications, Espoo, Finland, May 2003, pp. 399–405.

[17] A. Lönnqvist, J. Mallat, E. Noponen, J. Ala-Laurinaho, J. Säily, T. Koskinen, J. Häkli, and A. V. Räisänen, "A phase hologram compact RCS-range for scale model measurements," in *Proc. 3rd ESA Workshop on Millimetre Wave Technology and Applications*, Espoo, Finland, May 2003, pp. 511–515.

[18] E. Noponen, A. Lönnqvist, J. Säily, J. Häkli, T. Koskinen, V. Viikari, J. Ala-Laurinaho, J. Mallat, A. V. Räisänen, J. Salo, J. Meltaus, , and M. M. Salomaa, "Phase-type diffractive element for planar millimeter-wave generation at 310 GHz," in *Proc. Northern Optics 2003, The joint conference of the Optical Societies of Denmark, Finland, Norway and Sweden*, Espoo, Finland, June 2003, paper P097, p. 135.

[19] A. V. Räisänen, A. Lönnqvist, J. Mallat, E. Noponen, J. Ala-Laurinaho, J. Säily, T. Koskinen, and J. Häkli, "A compact RCS-range based on a phase hologram for scale model measurements at submm-wavelengths (invited plenary talk)," in *Proc. 11th Microcoll*, Budapest, Hungary, Sept. 2003, pp. 105–108.

[20] ——, "A compact RCS-range based on a phase hologram for scale model measurements at submm-wavelengths (invited plenary talk)," in *Proc. International Topical Meeting on Microwave Photonics, MWP2003*, Budapest, Hungary, Sept. 2003, pp. 55–58.

[21] A. V. Räisänen, J. Ala-Laurinaho, T. Koskinen, A. Lönnqvist, J. Säily, J. Häkli, J. Mallat, V. Viikari, S. Ranvier, and J. Tuovinen, "Computer-generated hologram and its use for submm-wave antenna measurement," in *2004 IEEE Aerospace Conference Proceedings*, Big Sky, MO, Mar. 2004, CD-ROM, ISBN: 0-7803-8156-4.

[22] A. V. Räisänen, T. Koskinen, A. Lönnqvist, J. Häkli, J. Ala-Laurinaho, J. Mallat, and J. Säily, "Recent results on using computer-generated submm-wave holograms for antenna and RCS measurements (invited paper)," in *MSMW'04 Symposium Proceedings, The Fifth International Kharkov Symposium on Physics and Engineering of Microwaves, Millimeter, and Submillimeter Waves*, Kharkov, Ukraine, June 2004, pp. 22–25.

[23] T. Koskinen, J. Ala-Laurinaho, and A. V. Räisänen, "Feasibility study of a hologram based compact antenna test range for 650 GHz," in *Proc. 26th Annual Antenna Measurement Techniques Association (AMTA) Meeting & Symposium*, Stone Mountain, GA, Oct. 2004, pp. 232–237.

[24] J. Häkli, J. Ala-Laurinaho, T. Koskinen, J. Lemanczyk, A. Lönnqvist, J. Mallat, A. V. Räisänen, J. Säily, J. Tuovinen, and V. Viikari, "Sub-mm antenna

tests in a hologram based CATR," in *Proc. 26th Annual Antenna Measurement Techniques Association (AMTA) Meeting & Symposium*, Stone Mountain, GA, Oct. 2004, pp. 238–242.

[25] J. Häkli, J. Ala-Laurinaho, T. Koskinen, A. Lönnqvist, J. Mallat, V. Viikari, J. Säily, A. V. Räisänen, J. Tuovinen, and J. Lemanczyk, "Mm- and submm wave hologram based compact antenna test ranges used for electrical antenna testing," in *Proc. 28th ESA Antenna Workshop on Space Antenna Systems and Technologies*, ESTEC, Noordwijk, The Netherlands, May 2005, pp. 385–392.

[26] A. Lönnqvist, J. Ala-Laurinaho, J. Häkli, T. Koskinen, J. Mallat, V. Viikari, and A. V. Räisänen, "Hologram based compact ranges for antenna and rcs testing at submm waves," in *Proc. ANTEM 2005 Conference*, Saint Malo, France, June 2005, pp. 222–223.

[27] J. Häkli, J. Ala-Laurinaho, T. Koskinen, J. Lemanczyk, A. Lönnqvist, J. Mallat, A. V. Räisänen, J. Säily, J. Tuovinen, and V. Viikari, "Sub-mm antenna tests in a hologram based CATR," *IEEE Antennas and Propagation Magazine*, vol. 47, no. 5, pp. 237–240, Apr. 2005.

[28] T. Koskinen, J. Häkli, J. Ala-Laurinaho, A. Lönnqvist, J. Mallat, V. Viikari, and A. V. Räisänen, "Reduction of cross-polarization in sub-millimetre-wave hologram-based CATR by using a polarization grid," in *Proc. 4th ESA Workshop on Millimetre Wave Technology and Applications*, Espoo, Finland, Feb. 2006, pp. 143–147.

[29] A. V. Räisänen, J. Ala-Laurinaho, J. Häkli, A. Karttunen, T. Koskinen, A. Lönnqvist, J. Mallat, E. Noponen, M. Vaaja, and V. Viikari, "Measurement of high-gain antennas at mm- and submm-wavelengths: challenges and solutions (invited plenary talk)," in *Proc. Antenna Measurement Techniques Association (AMTA) Europe Symposium*, Munich, Germany, May 2006, pp. 12–17.

[30] J. Häkli, T. Koskinen, J. Ala-Laurinaho, A. Karttunen, M. Vaaja, V. Viikari, A. Lönnqvist, J. Heinonen, J. Mallat, E. Noponen, P. Hautala, J. Lemanczyk, and A. V. Räisänen, "Development of a 650 GHz hologram based CATR for testing a 1.5 m reflector antenna," in *Proc. Antenna Measurement Techniques Association (AMTA) Europe Symposium*, Munich, Germany, May 2006, pp. 83–88.

[31] V. Viikari, J. Mallat, J. Ala-Laurinaho, J. Häkli, A. Karttunen, T. Koskinen, A. Lönnqvist, E. Noponen, M. Vaaja, and A. V. Räisänen, "New pattern correction techniques for submm-wave CATRs," in *Proc. European Conference on Antennas and Propagation (EuCAP)*, Nice, France, Nov. 2006, CD-ROM, ISBN: 92-9092-9375.

[32] J. Ala-Laurinaho, T. Koskinen, J. Häkli, A. Karttunen, A. Lönnqvist, E. Noponen, J. Mallat, M. Vaaja, V. Viikari, A. V. Räisänen, J. Heinonen, P. Hautala, and J. Lemanczyk, "Development of a hologram-based CATR for testing a very high gain antenna at 650 GHz," in *Proc. European Conference on Antennas and Propagation (EuCAP)*, Nice, France, Nov. 2006, CD-ROM, ISBN: 92-9092-9375.

[33] P. H. Siegel, "Terahertz technology," *IEEE Transactions on Microwave Theory and Techniques*, vol. 50, no. 3, pp. 910–928, Mar. 2002.

[34] P. de Maagt, "Terahertz technology for space and earth applications," in *Proc. European Conference on Antennas and Propagation (EuCAP)*, Nice, France, Nov. 2006, CD-ROM, ISBN: 92-9092-9375.

[35] T. G. Phillips and J. Keene, "Submillimeter astronomy," *Proceedings of the IEEE*, vol. 80, no. 11, pp. 1662–1678, Nov. 1992.

[36] A. van Ardenne, "Antennas for radio astronomy," in *Proc. European Conference on Antennas and Propagation (EuCAP)*, Nice, France, Nov. 2006, CD-ROM, ISBN: 92-9092-9375.

[37] (Last cited: May 29, 2007) MMA memo 187: Modeling of the submillimeter opacity on Chajnantor. [Online]. Available: http://www.alma.nrao.edu/memos/html-memos/alma187/memo187.html

[38] N. Erickson and V. Tolls, "Near-field measurements of the submillimeter wave astronomy satellite antenna," in *Proc. 20th ESTEC Antenna Workshop on Millimetre Wave Antenna Technology and Antenna Measurement*, ESTEC, Noordwijk, The Netherlands, June 1997, pp. 313–319.

[39] (Last cited: May 29, 2007) The submillimeter wave astronomy satellite (SWAS). [Online]. Available: http://www.cfa.harvard.edu/swas/

[40] U. Frisk, M. Hagström, J. Ala-Laurinaho, S. Andersson, J.-C. Berges, J.-P. Chabaud, M. Dahlgren, A. Emrich, H.-G. Florén, G. Florin, M. Fredrixon, T. Gaier, R. Haas, T. Hirvonen, Å. Hjalmarsson, B. Jakobsson, P. Jukkala, P. S. Kildal, E. Kollberg, J. Lassing, A. Lecacheux, P. Lehikoinen, A. Lehto, J. Mallat, C. Marty, D. Michet, J. Narbonne, M. Nexon, M. Olberg, A. O. H. Olofsson, G. Olofsson, A. Origné, M. Petersson, P. Piironen, R. Pons, D. Pouliquen, I. Ristorcelli, C. Rosolen, G. Rouaix, A. V. Räisänen, G. Serra, F. Sjöberg, L. Stenmark, S. Torchinsky, J. Tuovinen, C. Ullberg, E. Vinterhav, N. Wadefalk, H. Zirath, P. Zimmermann, and R. Zimmermann, "The Odin satellite, I. Radiometer design and test," *Astronomy & Astrophysics*, vol. 402, pp. L27–L34, 2003.

[41] V. Jamnejad, "A dual band telescope for microwave instrument on Rosetta orbiter (MIRO)," in *Proc. IEEE Aerospace Conference*, vol. 3, Aspen, CO, Mar. 1999, pp. 265–269.

[42] C. Alexander, S. Gulkis, M. Frerking, M. Janssen, D. Holmes, J. Burch, A. Stern, W. Gibson, R. Goldstein, J. Parker, J. Scherrer, D. Slater, S. Fuselier, and T. Gombosi, "The U.S. Rosetta project: NASA's contribution to the international Rosetta mission," in *Proc. IEEE Aerospace Conference*, Big Sky, MT, Mar. 2005, pp. 407–421.

[43] S. Dicker, P. Ade, J. Bock, J. Cung, E. Chapin, M. Devlin, M. Griffin, J. Gunderson, M. Halpern, P. Hargrave, D. Hughes, J. Klein, C. Mactavish, G. Marsden, P. Mauskopf, B. Netterfield, L. Olmi, M. Rex, D. Scott, G. Tucker, M. Truch, and M. Viero, "BLAST - A new balloon-borne submillimeter telescope," in *Proc. 13th International Symposium on Space Terahertz Technology*, Cambridge, MA, Mar. 2002, pp. 153–157.

[44] (Last cited: May 29, 2007) 'BLAST' off! Stratospheric telescope studies stars. [Online]. Available: http://www.space.com/scienceastronomy/050613_blast_launch.html

[45] M. V. Frank, "View through the door of the SOFIA project," *IEEE Transactions on Reliability*, vol. 54, no. 1, pp. 181–188, Mar. 2005.

[46] (Last cited: May 29, 2007) SOFIA Stratospheric observatory for infrared astronomy. [Online]. Available: http://www.sofia.usra.edu

[47] N. Mandolesi and F. Villa, "FIRST/Planck mission," in *Proc. 16th IEEE Instrumentation and Measurement Technology Conference (IMTC'99)*, vol. 2, Venice, Italy, May 1999, pp. 975–980.

[48] T. Stute, "The telescope reflectors for the ESA Planck mission," in *Proc. 28th ESA Antenna Workshop on Space Antenna Systems and Technologies*, vol. 2, Noordwijk, The Netherlands, May 2005, pp. 619–626.

[49] D. Leisawitz, T. Abel, R. Allen, D. Benford, A. Blain, C. Bombardelli, D. Calzetti, M. J. DiPirro, P. Ehrenfreund, N. Evans, J. Fischer, M. Harwit, T. T. Hyde, M. J. Kuchner, J. Leitner, E. Lorenzini, J. C. Mather, K. Menten, S. H. Moseley, L. G. Mundy, T. Nakagawa, D. Neufeld, S. A. Rinehart, J. Roman, S. Satyapal, R. F. Silverberg, H. P. Stahl, M. Swain, T. D. Swanson, W. Traub, E. L. Wright, and H. W. Yorke, "SPECS: The kilometer-baseline far-IR interferometer in NASA's space science roadmap," *Optical, Infrared, and Millimeter Space Telescopes, edited by John C. Mather, Proceedings of SPIE*, vol. 5487, pp. 1527–1537, 2004.

[50] D. Leisawitz, J. C. Mather, S. H. M. JR., and X. Zhang, "The submillimeter probe of the evolution of cosmic structure (SPECS)," *Astrophysics and Space Science*, vol. 269-270, pp. 563–567, 1999.

[51] D. Slater, P. Stek, R. Cofield, R. Dengler, J. Hardy, R. Jarnot, and R. Swindlehurst, "A large aperture 650 GHz near-field measurement system for the Earth observing system microwave limb sounder," in *Proc. 23rd*

Annual Meeting & Symposium of the Antenna Measurement Techniques Association (AMTA), Denver, CO, Oct. 2001, pp. 468–473.

[52] Y. Irimajiri, T. Manabe, S. Ochiai, H. Masuko, T. Yamagami, Y. Saito, N. Izutsu, T. Kawasaki, M. Namiki, and I. Murata, "BSMILES - A balloon-borne superconducting submillimeter-wave limb-emission sounder for stratospheric measurements," *IEEE Geoscience and Remote Sensing Letters*, vol. 3, no. 1, pp. 88–92, Jan. 2006.

[53] A. Murk, P. Yagoubov, U. Mair, M. Birk, G. Wagner, H. van de Stadt, R. Hoogeveen, and N. Kämpfer, "Antenna simulations for the THz and submm limb sounder TELIS," in *Proc. 28th ESA Antenna Workshop on Space Antenna Systems and Technologies*, vol. 2, Noordwijk, The Netherlands, May 2005, pp. 757–761.

[54] (Last cited: May 29, 2007) TELIS Terahertz limb sounder. [Online]. Available: http://www.dlr.de/caf/mf-ev/projekte/telis/telis_ge.html

[55] T. Manabe, "Development of superconducting submillimeter-wave limb-emission sounder (JEM/SMILES) aboard the International Space Station," *Journal of the Communications Research Laboratory*, vol. 49, no. 2, pp. 9–20, 2002.

[56] Y. J. Kasai, J. Urban, C. Takahashi, S. Hoshino, K. Takahashi, J. Inatani, M. Shiotani, and H. Masuko, "Stratospheric ozone isotope enrichment studied by submillimeter wave heterodyne radiometry: the observation capabilities of SMILES," *IEEE Transactions on Geoscience and Remote Sensing*, vol. 44, no. 3, pp. 676–693, Mar. 2006.

[57] R. J. Martin and D. H. Martin, "Quasi-optical antennas for radiometric remote-sensing," *Electronics & Communication Engineering Journal*, vol. 8, no. 1, pp. 37–48, Feb. 1996.

[58] C. Verdes, S. Bühler, A. von Engeln, T. Kuhn, K. Künzi, P. Eriksson, and B.-M. Sinnhuber, "Pointing and temperature retrieval from millimeter- submillimeter limb soundings," *Journal of Geohysical Research*, vol. 107, no. D16, pp. ACH 10 1–23, 2002.

[59] P. H. Nielsen, "Grating lobes from measured Planck telescope mirrors," in *Proc. 28th ESA Antenna Workshop on Space Antenna Systems and Technologies*, vol. 2, Noordwijk, The Netherlands, May 2005, pp. 627–631.

[60] R. C. Johnson, H. A. Ecker, and R. A. Moore, "Compact range techniques and measurements," *IEEE Transactions on Antennas and Propagation*, vol. 17, no. 5, pp. 568–576, Sept. 1969.

[61] P. R. Foster, D. Martin, C. Parini, A. V. Räisänen, J. Ala-Laurinaho, T. Hirvonen, A. Lehto, T. Sehm, J. Tuovinen, F. Jensen, and K. Pontoppidan,

Mmwave antenna testing techniques - Phase 2. MAAS Report 304, Issue No. 2, ESTEC Contract No. 11641/95/NL/PB(SC), Dec. 1996, p. 224.

[62] J. Tuovinen, "Methods for testing reflector antennas at 1 THz," *IEEE Antennas and Propagation Magazine*, vol. 35, no. 6, pp. 7–13, Dec. 1993.

[63] T. Hirvonen, J. P. S. Ala-Laurinaho, J. Tuovinen, and A. V. Räisänen, "A compact antenna test range based on a hologram," *IEEE Transactions on Antennas and Propagation*, vol. 45, no. 8, pp. 1270–1276, Aug. 1997.

[64] T. Sehm, J. Ala-Laurinaho, T. Hirvonen, and A. V. Räisänen, "Antenna measurements using a hologram CATR," *Electronics Letters*, vol. 35, no. 10, pp. 757–758, May 1999.

[65] J. Ala-Laurinaho, T. Hirvonen, P. Piironen, A. Lehto, J. Tuovinen, A. V. Räisänen, and U. Frisk, "Measurement of the Odin telescope at 119 GHz with a hologram-type CATR," *IEEE Transactions on Antennas and Propagation*, vol. 49, no. 9, pp. 1264–1270, Sept. 2001.

[66] J. H. Bryant, "The first century of microwaves – 1886 to 1986," *IEEE Transactions on Microwave Theory and Techniques*, vol. 36, no. 5, pp. 830–858, May 1988.

[67] C. A. Balanis, *Antenna theory analysis and design, 2nd ed.* New York: John Wiley & Sons, Inc., 1997, p. 941.

[68] W. L. Stutzman and G. A. Thiele, *Antenna theory and design.* New York: John Wiley & Sons, Inc., 1981, p. 598.

[69] *IEEE Standard definitions of terms for antennas*, IEEE Std 145-1993, published by IEEE, Inc., 1993, p. 36.

[70] A. D. Yaghjian, "An overview of near-field antenna measurements," *IEEE Transactions on Antennas and Propagation*, vol. 34, no. 1, pp. 30–45, Jan. 1986.

[71] *IEEE Standard test procedure for antennas*, IEEE Std 149-1979, published by IEEE, Inc., distributed by Wiley-Interscience, 1979, p. 143.

[72] G. E. Evans, *Antenna measurement techniques.* Norwood, MA: Artech House, 1990, p. 229.

[73] R. C. Hansen, "Measurement distance effects on low sidelobe patterns," *IEEE Transactions on Antennas and Propagation*, vol. 32, no. 6, pp. 591–594, June 1984.

[74] W. H. Kummer and E. S. Gillespie, "Antenna measurements - 1978," *Proceedings of the IEEE*, vol. 66, no. 4, pp. 483–507, Apr. 1978.

[75] Y. Rahmat-Samii, L. I. Williams, and R. G. Yaccarino, "The UCLA bipolar planar-near-field antenna-measurement and diagnostics range," *IEEE Antennas and Propagation Magazine*, vol. 37, no. 6, pp. 16–35, Dec. 1995.

[76] A. C. Newell, "Error analysis techniques for planar near-field measurements," *IEEE Transactions on Antennas and Propagation*, vol. 36, no. 6, pp. 754–768, June 1988.

[77] J. Tuovinen, A. Lehto, and A. Räisänen, "A new method for correcting phase errors caused by flexing of cables in antenna measurements," *IEEE Transactions on Antennas and Propagation*, vol. 39, no. 6, pp. 859–861, June 1991.

[78] J. Säily, P. Eskelinen, and A. V. Räisänen, "Pilot signal based real-time measurement and correction of phase errors caused by microwave cable flexing in planar near-field tests," *IEEE Transactions on Antennas and Propagation*, vol. 51, no. 2, pp. 195–200, Feb. 2003.

[79] A. von Lerber, V. Viikari, A. Liseno, J. Ala-Laurinaho, and A. V. Räisänen, "A feasibility study of phase retrieval algorithms at submillimeter wavelengths," in *Proc. 27th Annual Antenna Measurement Techniques Association (AMTA) Meeting & Symposium*, Newport, RI, Oct. 2005, pp. 79–84.

[80] S. F. Razavi and Y. Rahmat-Samii, "A new look at phaseless planar near field measurements: limitations, simulations, measurements and a hybrid solution," in *Proc. 28th Annual Antenna Measurement Techniques Association (AMTA) Meeting & Symposium*, Austin, TX, Oct. 2006, pp. 26–31.

[81] A. D. Olver, "Compact antenna test ranges," in *Proc. International Conference on Antennas and Propagation ICAP*, York, UK, 1991, pp. 99–109.

[82] J. Hartmann, J. Habersack, H.-J. Steiner, J. Lemanczyk, and P. D. Maagt, "Calibration and verification measurements in compensated compact ranges up to 500 GHz," in *Proc. 23rd Annual Meeting & Symposium of the Antenna Measurement Techniques Association (AMTA)*, Denver, CO, Oct. 2001, pp. 377–382.

[83] C. G. Parini and C. J. Prior, "Radiation pattern measurements of electrically large antennas using a compact antenna test range at 180 GHz," *Electronics Letters*, vol. 24, no. 25, pp. 1552–1554, Dec. 1988.

[84] J. R. Descardeci and C. G. Parini, "Trireflector compact antenna test range," *Proc. IEE Microwaves, Antennas and Propagation*, vol. 144, no. 5, pp. 305–310, Oct. 1997.

[85] C. Rieckmann, M. R. Rayner, and C. G. Parini, "Optimisation of cross-polarisation performance for tri-reflector CATR with spherical main reflector," *Electronics Letters*, vol. 35, no. 17, pp. 1403–1404, Aug. 1999.

[86] T.-H. Lee and W. D. Burnside, "Performance trade-off between serrated edge and blended rolled edge compact range reflectors," *IEEE Transactions on Antennas and Propagation*, vol. 44, no. 1, pp. 87–96, Jan. 1996.

[87] M. S. A. Mahmoud, T.-H. Lee, and W. D. Burnside, "Enhanced compact range reflector concept using an R-card fence: two-dimensional case," *IEEE Transactions on Antennas and Propagation*, vol. 49, no. 3, pp. 419–428, Mar. 2001.

[88] H. Garcia, G. Forma, C. Nardini, D. Dubruel, J. M. Canales, and M. Paquay, "Characterisation of the Planck radio frequency qualification model and preparations for flight model tests," in *Proc. 28th Annual Antenna Measurement Techniques Association (AMTA) Meeting & Symposium*, Austin, TX, Oct. 2006, pp. 358–363.

[89] J. Habersack, J. Hartmann, J. Lemanczyk, P. D. Maagt, and H.-J. Steiner, "Facility trade-off for measurements up to 500 GHz," in *Proc. 23rd Annual Meeting & Symposium of the Antenna Measurement Techniques Association (AMTA)*, Denver, CO, Oct. 2001, pp. 261–266.

[90] K. Miyata, "A 12 GHz-band planar waveguide array antenna for compact range application- a preliminary study," *IEEE Transactions on Antennas and Propagation*, vol. 44, no. 4, pp. 588–589, Apr. 1996.

[91] (Last cited: May 29, 2007) Holography. [Online]. Available: http://en.wikipedia.org/wiki/Holography

[92] W.-H. Lee, "Computer-generated holograms: techniques and applications," *Progress in Optics XVI, E. Wolf, Ed., Amsterdam, The Netherlands: Elsevier*, pp. 121–231, 1978.

[93] T. Sehm, T. Hirvonen, J. Ala-Laurinaho, and A. V. Räisänen, "Measurement of a novel 40 GHz planar antenna using planar near-field scanning techniques and a hologram CATR," in *Proc. 27th European Microwave Conference*, Jerusalem, Israel, Sept. 1997, pp. 880–885.

[94] J. Säily, J. Ala-Laurinaho, J. Häkli, J. Tuovinen, A. Lehto, and A. V. Räisänen, "Test results of 310 GHz hologram compact antenna test range," *Electronics Letters*, vol. 36, no. 2, pp. 111–112, Jan. 2000.

[95] A. Vasara, J. Turunen, and A. T. Friberg, "Realization of general nondiffracting beams with computer-generated holograms," *Journal of Optical Society of America A*, vol. 6, no. 11, pp. 1748–1754, Nov. 1989.

[96] A. Lönnqvist, J. Mallat, and A. V. Räisänen, "Phase-hologram-based compact RCS test range at 310 GHz for scale models," *IEEE Transactions on Microwave Theory and Techniques*, vol. 54, no. 6, pp. 2391–2397, June 2006.

[97] K. S. Yee, "Numerical solution of initial boundary value problems involving Maxwell's equations in isotropic media," *IEEE Transactions on Antennas and Propagation*, vol. 14, no. 3, pp. 302–307, May 1966.

[98] A. Taflove and S. C. Hagness, *Computational Electrodynamics: The Finite-Difference Time-Domain Method, 3rd ed.* Norwood, MA: Artech House, 2005, p. 1006.

[99] J. Ala-Laurinaho, "Numerical studies on a radio frequency hologram and its use in antenna measurements," Ph.D. dissertation, Helsinki University of Technology, Espoo, Finland, 2001.

[100] J. Ala-Laurinaho, T. Hirvonen, J. Tuovinen, and A. V. Räisänen, "Numerical modeling of a nonuniform grating with FDTD," *Microwave and Optical Technology Letters*, vol. 15, no. 3, pp. 134–139, June 1997.

[101] J. Ala-Laurinaho, T. Sehm, J. Säily, and A. V. Räisänen, "Cross-polarization performance of the hologram compact antenna test range," *Microwave and Optical Technology Letters*, vol. 27, no. 4, pp. 225–229, Nov. 2000.

[102] J.-P. Berenger, "A perfectly matched layer for the absorption of electromagnetic waves," *Journal of Computational Physics*, vol. 114, no. 2, pp. 185–200, Oct. 1994.

[103] C. M. Furse, S. P. Mathur, and O. P. Gandhi, "Improvements to the finite-difference time-domain method for calculating the radar cross section of a perfectly conducting target," *IEEE Transactions on Microwave Theory and Techniques*, vol. 38, no. 7, pp. 919–927, July 1990.

[104] C. M. Furse, D. H. Roper, D. N. Buechler, D. A. Christensen, and C. H. Durney, "The problem and treatment of DC offsets in FDTD simulations," *IEEE Transactions on Microwave Theory and Techniques*, vol. 48, no. 8, pp. 1198–1201, Aug. 2000.

[105] F. Sobel, F. L. Wentworth, and J. C. Wiltse, "Quasi-optical surface waveguide and other components for 100- to 300-Gc region," *IRE Transactions on Microwave Theory and Techniques*, vol. MTT-9, no. 6, pp. 512–518, Nov. 1961.

[106] J. W. Lamb, "Miscellaneous data on materials for millimetre and submillimetre optics," *International Journal of Infrared and Millimeter Waves*, vol. 17, no. 12, pp. 1997–2034, 1996.

[107] J. D. Jackson, *Classical Electrodynamics, 3rd ed.* New York: John Wiley & Sons, Inc., 1999, p. 808.

[108] J. Ala-Laurinaho, T. Hirvonen, and A. V. Räisänen, "On the planarity errors of the hologram of the CATR," in *Proc. IEEE Antennas and Propagation International Symposium*, Orlando, FL, July 1999, pp. 2166–2169.

[109] J. Ala-Laurinaho, J. Mallat, V. Viikari, and A. V. Räisänen, "Dielectric-loaded flat reflector test antenna for submillimetre wavelengths," in *Proc. ANTEM 2005 Conference*, Saint Malo, France, June 2005, pp. 260–261.

[110] J. Häkli, J. Ala-Laurinaho, and A. V. Räisänen, "A numerical synthesis method for designing a shaped dual reflector feed system," *Proc. IEE Microwaves, Antennas and Propagation*, vol. 152, no. 5, pp. 311–318, Oct. 2005.

[111] J. Häkli, "Shaped reflector antenna design and antenna measurements at sub-mm wavelengths," Ph.D. dissertation, Helsinki University of Technology, Espoo, Finland, 2006.

HELSINKI UNIVERSITY OF TECHNOLOGY RADIO LABORATORY REPORTS

S 275 Räisänen, A.V., Lindberg, S.
TKK Radio Laboratory research and education 2005, March 2006

S 276 Salonen, I.
Evaluation and compensation of mutual coupling and other non-idealities in small antenna arrays, May 2006

S 277 Suvikunnas,P., Salo, J., Vuokko, L., Sulonen, K., Vainikainen, P.
Comparison of MIMO antenna configurations: Methods and experimental results, June 2006

S 278 Salo, J.
Statistical analysis of the wireless propagation channel and its mutual information, July 2006

S 279 Suvikunnas, P.
Methods and criteria for performance analysis of multiantenna systems in mobile communications, August 2006

S 280 Tretyakov, S., Alitalo, P.
International student seminar on microwave applications of novel physical phenomena, August 2006

S 281 Häkli, J.
Shaped reflector antenna design and antenna measurements at sub-mm wavelengths, September 2006

S 282 Lönnqvist, A.
Applications of hologram-based compact range: Antenna radiation pattern, radar cross section, and absorber reflectivity measurement, September 2006

S 283 Tretyakov, S., Osipov, A.
Applied theory of electromagnetic scattering and diffraction, September 2006

S 284 Belov, P.
Analytical modelling of metamaterials and a new principle of sub-wavelength imaging, September 2006

S 285 Ikonen, P.
Artificial electromagnetic composite structures in selected microwave applications, March 2007

S 286 Räisänen, A.V., Lindberg, S.
TKK Radio Laboratory research and education 2006, March 2007

S 287 Viikari, V.
Antenna pattern correction techniques at submillimeter wavelengths, April 2007

S 288 Villanen, J., Suvikunnas, P., Icheln, C., Ollikainen, J., Vainikainen, P.
Performance analysis and design aspects of mobile terminal multi-antenna configurations, May 2007

ISBN 978-951-22-8795-6
ISSN 1456-3835